MINISTERE DE L'ENSEIGNEMENT SUPERIEUR
ET DE LA RECHERCHE SCIENTIFIQUE

Felix Houphouet-Boigny University

UNITE DE FORMATION ET DE RECHERCHE SCIENCES DES STRUCTURES DE LA MATIERE ET DE TECHNOLOGIE

RÉPUBLIQUE DE CÔTE D'IVOIRE
UNION - DISCIPLINE - TRAVAIL

N°: 832

SPONSORED BY THE Federal Ministry of Education and Research

INTERNATIONAL MASTER PROGRAM IN ENERGY AND GREEN HYDROGEN

SPECIALITY: GEORESOURCES (WIND AND WATER) TECHNOLOGY

MASTER THESIS

Subject/Topic:

Implication of Wind Speed Data variant for Wind Power Simulation

Presented on the 25th September 2025 and by:

Adovi Fulbert Richcarlos EDOH

Jury Members:

Prof. Kouadio Olivier OBROU	**President**
Dr. Daouda KONE	**Examiner**
Dr. Kamenan Blaise KOUA	**Supervisor**
Prof. Harrie-Jan HENDRICKS-FRANSSEN	**Co-Supervisor**
Dr. Shuying CHEN	**Co-Supervisor**

Academic year 2024-2025

DEDICATION

"To my son and my whole family"

ACKNOWLEGMENT

Foremost, I would like to praise the almighty for his wonders in my life and for his assistance throughout this achievement.

All my gratitude to the German Federal Ministry of Education and Research (BMBF) for their financial support of this program and to the West African Science Service Centre for Climate Change and Adapted Land Use (WASCAL) for awarding me this scholarship, which has enhanced my academic career.

My thank to the President of Université Félix Houphouët Boigny Prof. Ballo ZIE, to the President of Université de Lome Prof. Adama Mawulé KPODAR, and to the President of Université Abdou Moumouni Prof. Baragé MOUSSA.

I would like to thank the vice Chancellor of Forschungszentrum Jülich and the Director of the institute IBG3 where I complete the 6 months of my internship.

My thank also to the Director of GSP Togo Prof Komi AGBOKA at Université de Lomé, to the Director of GSP Niger Prof. Adamou RABBANI at Université Abdou Moumouni, to the Director Prof. Edouard KOUASSI of GSP Cote d'Ivoire, and to the Coordinator of the H2 Program at the GSP Cote d'Ivoire Dr Wanignon Ferdinand FASSINOU.

I am grateful to my major supervisor Dr. Kamenan Blaise KOUA and to my co-supervisors Prof. Harrie-Jan HENDRICKS-FRANSSEN and Dr. Shuying CHEN for their significant contribution to the success of this thesis.

I extend my thanks to the President of the Jury Prof. Kouadio Olivier OBROU and to the Jury Examiner Dr. Daouda KONE.

And at last, but not the least, my thank to Dr. Bamidele OLORUNTOBA for facilitating my integration in Germany during my internship, to all my colleagues of IMP-EGH batch 2, to all my colleagues of track Georesources, to Mr. Hèzyèwè TANGOU, to Mr. Komlan WOENAGNON, to Mr. Bagnabana KONGA, to Mrs. Imelda AKUE-GOEH, to Mrs. Abiré PAGOUSOOU, to Mr. Jean Didier KOUAKOU, to Mr. Amidou TIEMTORE, to Mr Hervé KOUADIO, and to Mr Stephane BROU.

All the above have impacted this success by their support, encouragement, guidance, which contributes to my academic and professional growth. Thank you all.

ABSTRACT

With the need for a shift from the use of fossil fuels to renewable energy, wind technology is one of the promising, clean, renewable, and cost-effective energy sources. For sub-Saharan regions where 600 million people still lack electricity, wind energy appears to be an opportunity to assure energy security especially, in southern Africa, where abundant wind energy potential exists. Basically, wind technology consists of the use of a wind turbine, which extracts the kinetic energy of moving air through a rotor. This implies the knowledge of wind speed at the rotor level, known as Hub height (around 100m), but wind measurements are typically done at ground level (around 10m). Therefore, it is crucial to find alternative ways for wind data assessment at the rotor level. Numerical atmospheric datasets and height scaling methods seem to be solutions. This study evaluates the impact of using different height scaling methods with and without numerical atmospheric datasets, the high-resolution ICON in Limited Area Mode (ICON-LAM), the ERA5 reanalysis, and the statistical downscaling variant of ERA5 (ERA5_GWA) on the multiple heights wind speed calculation and subsequently, on the wind power estimation over southern Africa from 2017 to 2019. The results show that ERA5_GWA outperforms ERA5 and ICON-LAM for the 10m wind speed simulation. ERA5 introduced the highest bias with an underestimation of the wind power at 20m, 40m and 60m, regardless of the used wind speed height scaling method. Most of the scaling methods performed similarly except for the Justus_Law, which introduced an overestimation of the wind power, and the Linear interpolation, which introduced an underestimation. The accuracy of scaling methods using vertical levels of wind speed from numerical atmospheric datasets is highly dependent on the choices of the nearest levels close to the target height wind speed. This study reveals that the choice of datasets has a greater impact than wind speed height scaling on wind energy assessment.

Keywords: ICON-LAM; ERA5; Global Wind Atlas; Wind Speed; Height Scaling; Wind Power; Africa.

RESUMÉ

Avec la nécessité de passer des combustibles fossiles aux énergies renouvelables, la technologie éolienne est l'une des sources d'énergie prometteuses, propres, renouvelables et rentables. Pour les régions subsahariennes où 600 millions de personnes n'ont toujours pas accès à l'électricité, l'énergie éolienne semble être une opportunité d'assurer la sécurité énergétique, en particulier en Afrique australe, où le potentiel éolien est abondant. Fondamentalement, la technologie éolienne consiste à utiliser une éolienne qui extrait l'énergie cinétique de l'air en mouvement à l'aide d'un rotor. Cela implique de connaître la vitesse du vent au niveau du rotor, appelée hauteur de moyeu (environ 100 m), mais les mesures du vent sont généralement effectuées au niveau du sol (environ 10 m). Il est donc essentiel de trouver d'autres moyens d'évaluer les données éoliennes au niveau du rotor. Les ensembles de données atmosphériques numériques et les méthodes de mise à l'échelle en hauteur semblent être des solutions. Cette étude évalue l'impact de l'utilisation de différentes méthodes de mise à l'échelle en hauteur avec et sans ensembles de données atmosphériques numériques, à savoir le modèle ICON haute résolution en mode zone limitée (ICON-LAM), la réanalyse ERA5 et la variante de réduction d'échelle statistique de l'ERA5 (ERA5_GWA) sur le calcul de la vitesse du vent à plusieurs hauteurs et, par conséquent, sur l'estimation de la puissance éolienne en Afrique australe de 2017 à 2019. Les résultats de l'évaluation montrent que ERA5_GWA a une meilleure représentation de la vitesse du vent a 10m comparé á ERA5 et ICON-LAM entre 2017 et 2019 dans la partie australe de l'Afrique. ERA5 introduit un biais plus élevé avec une sous-estimation de la puissance éolienne à 20 m, 40 m et 60 m, quelle que soit la méthode utilisée pour la mise à l'échelle de la vitesse du vent. La plupart des méthodes de mise à l'échelle ont donné des résultats similaires, à l'exception de la méthode Justus_Law, qui a introduit une surestimation de la puissance éolienne, et de l'interpolation linéaire, qui a son niveau a introduit une sous-estimation. La précision des méthodes de mise à l'échelle utilisant les niveaux verticaux de vitesse du vent provenant des ensembles de données atmosphériques numériques dépend fortement du choix des niveaux les plus proches de la hauteur cible. Cette étude révèle que le choix des ensembles de données a un impact plus important que les méthodes de mise à l'échelle de la vitesse du vent lors de l'estimation de l'énergie éolienne.

Mots-clés : ICON-LAM ; ERA5 ; Atlas mondial des vents ; Vitesse du vent ; Mise à l'échelle en fonction de la hauteur ; Énergie éolienne ; Afrique.

ACRONYMS AND ABBREVIATIONS

3D-Var	: Three-Dimensional Variational
4D-Var	: Four-Dimensional Variational
20CRv3	: Twentieth Century Reanalysis, version 3
AREI	: African Renewable Energy Initiative
C3S	: Copernicus Climate Change Service
CERRA	: Copernicus Regional ReAnalysis
CFSv2	: Climate Forecast System, version 2
CIRES	: Cooperative Institute for Research in Environmental Sciences
COSMO-REA6	: Consortium for Small-scale Modelling – Regional ReAnalysis at 6 km resolution
CSFR	: Climate Forecast System Reanalysis
DOE	: Department of Energy
DWD	: Deutscher Wetterdienst
ECMWF	: European Centre for Medium-Range Weather Forecasts
ERA5	: ECMWF Reanalysis 5
ERA5_GWA	: ECMWF Reanalysis 5 Global Wind Atlas
ERA-Int	: ECMWF Reanalysis interim
ESA-CCI	: European Space Agency Climate Change Initiative
GHG	: GreenHouses Gas
HAWTs	: Horizontal Axis Wind Turbines
ICON-LAM	: ICOsahedral Non-hydrostatic in Limited Area Mode
IEA	: International Energy Agency
IRENA	: International Renewable ENergy Agency
JRA-55	: Japanese Reanalysis 55
LiDAR	: Light Detection And Ranging
MAE	: Mean Absolute Error
ME	: Mean Error
MERRA-2	: Modern-Era Retrospective analysis for Research and Applications Version 2
MPI-M	: Max-Planck-Institut für Meteorologie
NASA	: National Aeronautics and Space Administration

NCAR : National Center for Atmospheric Research

NCEI_ISD : National Center for Environmental Information Integrated Surface Database

NCEP : National Center for Environmental Prediction

NOAA : National Oceanic and Atmospheric Administration

PSS : Perkins Skill Score

RESKit : Renewable Energy Simulation toolKit

SAR : Synthetic Aperture Radar

SASSCAL_WN ` : Southern African Science Service Centre for Climate Change and Adaptive Land Management Weather Net

TAHMO : Trans-African Hydro-Meteorological Observatory

VAWTs : Vertical Axis Wind Turbines

WASA : Wind Atlas of South Africa

WRF : Weather Research and Forecasting

LIST OF TABLES

LIST OF FIGURES

TABLES OF CONTENTS

GENERAL INTRODUCTION

INTRODUCTION

The contemporary world is experiencing an increase in population, which is projected to reach 9.7 billion by 2050, and this, eventually, will lead to a corresponding global energy demand increase (Gerland et al., 2022). Fossil fuels, including coal, oil and natural gas, account for more than 80% of the global energy supply (Holechek et al., 2022) as shown in Figure 1 (Energy Institute, 2025). It is evident that the energy sector is a significant contributor to climate change, with the various methods of utilising fossil fuels being a primary factor in greenhouse gas (GHG) emissions (IEA, 2025a). Despite its negligible contribution to greenhouse gas emissions, the African continent is one of the most affected by the effects of climate change, due to its vulnerability, lack of resilience, and limited mitigation efforts (Trisos et al., 2022). Moreover, in sub-Saharan Africa, it is estimated that approximately 600 million people still lack access to electricity (IEA, 2025b), and the African continent has also been subject to a series of extreme weather events and ongoing energy poverty (Nhamo et al., 2025). Therefore, there is an urgent necessity to shift from fossil fuels to renewable energy sources.

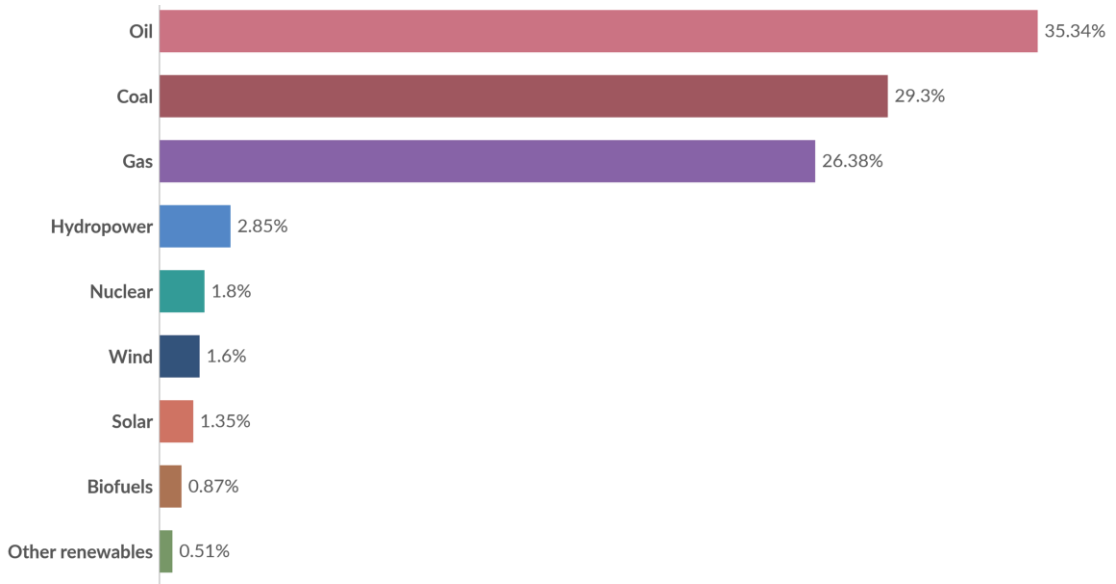

Figure 1: World Share of direct primary energy consumption by source in 2024 (Energy Institute, 2025)

Wind energy is a promising renewable energy source offering significant advantages since it is environmentally clean, sustainable, and has seen efficiency improvement and cost has

dropped substantially over time (Kara & Sahin, 2023). This makes it an attractive choice for future energy needs. Wind turbines harness the kinetic energy of the wind by turning a rotor, relying on varying wind speed, which fluctuates both spatially and temporally (Gumuła et al., 2017). Therefore, the knowledge of reliable wind resources at the rotor level is fundamental to energy policy planning and wind project development. However, standard wind measurements are taken at low heights below the rotor and close to the ground (Barthelmie et al., 2016).

The use of atmospheric numerical datasets to assess the wind resources for downstream wind energy applications is one solution to measurement issues. These atmospheric numerical datasets are simulated products, and their output data influence the estimation of wind energy (Emeis, 2018). Between these simulated datasets, we distinguished the fifth version of the ECMWF reanalysis (ERA5) dataset, the ERA5_Global Wind Atlas (ERA5_GWA), which is a statistical downscaling variant of ERA5, and the ICOsahedral Non-hydrostatic Limited Area Model (ICON-LAM), which is a dynamical downscaling dataset (Chen et al., 2024b). Despite continuous improvements to the many available simulated wind datasets, significant questions remain about their reliability for wind power simulation. Another approach to addressing measurement issues is to use extrapolation techniques to estimate the wind speed at the turbine rotor level from a given measurement height. These techniques, known as height scaling methods, are tools that have assumptions, such as the surface roughness length, which depend heavily on land cover. Especially in regions with sparse data, the assumptions of height scaling methods are often poorly defined, which can affect the accuracy of wind energy estimation. Consequently, the deployment of wind energy technology is limited in such regions, for example, Southern Africa. Due to all these unknowns, it is crucial to evaluate how different wind speed data variant affects the estimation of wind energy production in Southern Africa, a region with abundant wind potential.

The evaluation of wind speed data comes with several questions. How do height scaling methods affect the wind speed estimation? What is the impact of dataset variability on the wind power simulation? And to what extent do wind speed datasets and height scaling models influence the accuracy of wind power simulations in Southern Africa? Answering those questions help to understand the impact of dataset and scaling methods on wind energy estimation.

One hypothesis is that the height scaling methods introduce new uncertainty in wind speed estimation since these methods are designed for a specific weather condition and the type of terrain. Another hypothesis is that using different simulated datasets leads to different wind power estimations for the same location under the same conditions.

Therefore, this study aims to evaluate the impact of different datasets and height scaling methods on wind power estimation, through three main objectives, which will help policymakers and future wind projects in the region. The first objective is to compare the simulated 10 m wind speeds from the ERA5 reanalysis dataset, the ERA5_GWA statistical downscaling dataset, and the ICON-LAM dynamical downscaling dataset against in-situ 10m wind speed from over more than 200 stations in southern Africa for a validation. The second objective is to evaluate the influence of different height scaling methods on the accuracy of the scaled wind speeds at various hub heights. The last objective is to quantify the combined impact of the datasets and the height scaling methods on the simulated wind power.

The first section of this study is a bibliographic review. It begins with the history and the background of wind technology. A comprehensive review of existing literature on wind resource assessment, atmospheric numerical datasets, height scaling methods, and wind energy estimation will help to identify any gaps and limitations in the current wind power generation technology.

The second section is the Materials and Methods section. This section includes the location of the study site. It also includes a description of models used and how they were employed. All the metrics and tools involved in the analysis are presented.

In the next section Results and Discussion, the results of the dataset performance at 10m, the height scaling methods evaluation, and the estimation of wind energy by method and dataset are presented and discussed.

Finally, in Conclusion and Perspectives section, a summary of the entire study is provided. Then, recommendations for future study directions are highlighted for further improvement of the study.

CHAPTER I: LITERATURE REVIEW

CHAPTER I: LITERATURE REVIEW

Introduction

This chapter starts with the background of wind technology in which the history and the development of wind technology are presented. The chapter continues with a review of the wind resources, the resource assessment, the atmospheric numerical models, and the scaling methods. Finally, the chapter ends with a gap analysis, which helps to identify the lack of existing studies.

I.1. History and Development of Wind Energy

The use of wind power is not a new thought. The wind technology was not primarily developed for generating electricity, but rather for milling and pumping purposes (Kaldellis & Zafirakis, 2011). One of the earliest windmills, a machine that utilises wind power, was discovered in ancient Persia, nowadays known as eastern Iran, around the 10th century (Pasqualetti et al., 2004). In Europe, it was later in the 12th century that windmills became common, particularly in northern countries such as the Netherlands and England, where they were used in agriculture and industry for many years (Fleming & Probert, 1984). It was finally at the end of the 19th century that Charles F. Brush in Cleveland, Ohio, built the first larger automatically operated wind turbine, which generated electricity with a power of 12kW (Burton et al., 2011). Brush's wind turbine demonstrates its ability to convert the power of the wind into electricity. Figure 2 shows the illustration of Brush's Wind turbine (Righter, 1996).

The oil crisis in the second half of the 20th century, combined with the development of technology in the fields of aerodynamics, power electronics, and material sciences, contributed greatly to the fast evolution of wind turbine design and subsequently stimulated investment and innovation in renewable energies, including wind power (Thomas & Robbins, 1980). Denmark, like a pioneer, played a key role in the commercialisation of wind power by exporting wind turbines, especially to the United States and initiated a deployment of grid-connected wind turbines (Gipe, 1991). With the improvement of turbine efficiency, policies which support the global wind energy sector, environmental energy security and climate change issues, has been exponentially growing since the 2000s. The world's global wind power installed capacity moves from just over 17GW to more than 1,100 GW in 2024 (IRENA, 2025), and then wind energy is one of the fastest-growing

renewable sources of electricity.

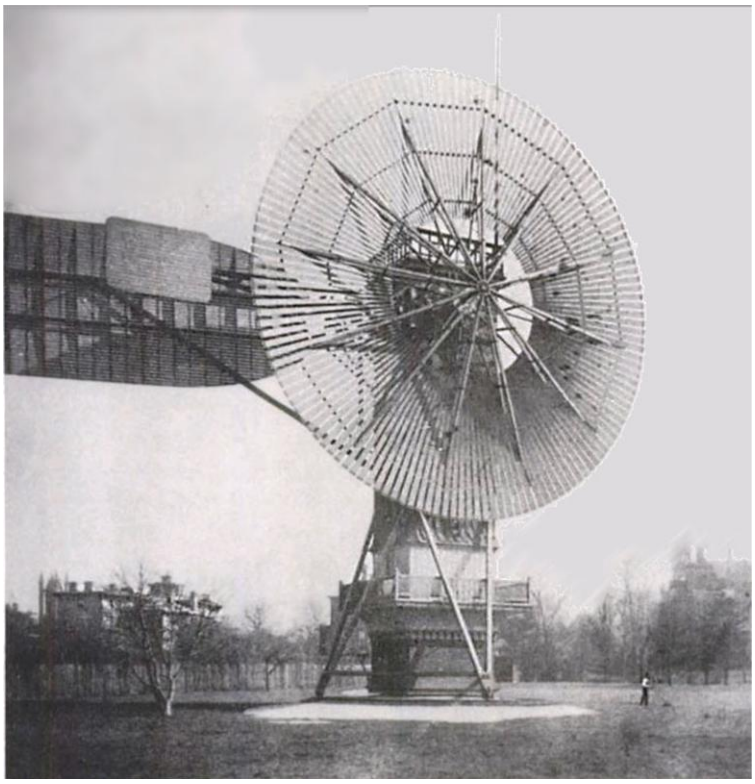

Figure 2 : Brush's wind turbine (Righter, 1996)

Nowadays, wind turbines are in the range of megawatt installed capacity with a hub height exceeding 100 meters and over 150 meters rotor diameters compared to a few kilowatts with small meter heights and diameters in their early stage. Otherwise, increasingly offshore wind turbines are emerging due to the more consistent and higher offshore wind, but onshore wind turbines are the most installed to date.

I.2. Wind Technology

I.2.1. The wind turbine

A wind turbine is the main technology of wind power generation. It can be onshore or offshore, depending on whether it is installed on land or at sea. Onshore wind turbines are considered the most mature segment of wind power due to their long deployment history, lower installation costs, and well-established infrastructure compared to offshore alternatives (Tumse et al., 2024), but suffer from land availability and turbulence. On the other hand, offshore wind systems have the advantage of higher and stable wind speeds but face complex installation, maintenance, and grid connection challenges.

Based on the rotor axes orientation, we can distinguish two principal types of turbines: The Horizontal Axis Wind Turbines (HAWTs) and the Vertical Axis Wind Turbines (VAWTs). HAWTs' rotor shafts are aligned horizontally and face into the wind, then use pitch and yaw mechanisms for control (Elkodama et al., 2023), which led them to a higher aerodynamic efficiency and made them the most commercially viable wind turbine. On the opposite side, VAWTs' rotors are aligned vertically and benefit from their ground-level gearbox placement, which is useful for maintenance purposes, but they have lower aerodynamic efficiency and higher fatigue loads (Ghoneam et al., 2024). A typical HAWT and VAWT is illustrated in Figure 3 (Rashad et al., 2017).

Figure 3 : Illustration of Typical HAWT (A) and VAWT (B) (Rashad et al., 2017)

According to the size, we have small wind turbines with an installed capacity up to 40kW, medium wind turbines with an installed capacity in the range of 40kW to 1MW, large wind turbines with an installed capacity of 1MW to 10MW and ultra-large wind turbines for more than 10MW (Kassa et al., 2024). The size of a wind turbine is influenced by some characteristics, such as the hub height and the rotor's diameter. The more the rotor's diameter and the hub height are, the better the wind turbine can harvest wind energy, because a higher hub height gives access to stronger winds and longer rotor blades increase the swept area of the rotor (Lee et al., 2019). Figure 4 shows the basic main part of a wind turbine (Aminzadeh et al., 2023). Additional parameters are the control system and the

advanced material used. Advanced materials like carbon composite and a digitalised control system help to optimise the performance of the turbine as they allow a great bending strength of the blades and a good wind capture (Tolasa & Furi, 2025).

Nowadays, wind turbines are typically from medium range to ultra large, using a bigger rotor diameter and hub height, and are built with advanced materials and digitalised control systems. All those improvements in technology help to improve not only the overall efficiency but also reduce the construction and maintenance costs. Therefore, wind technology becomes more competitive with fossil fuels (Mehta et al., 2024). However, with all those improvements, the speed at which wind blows throughout the rotors remains the most critical factor for a wind turbine operation.

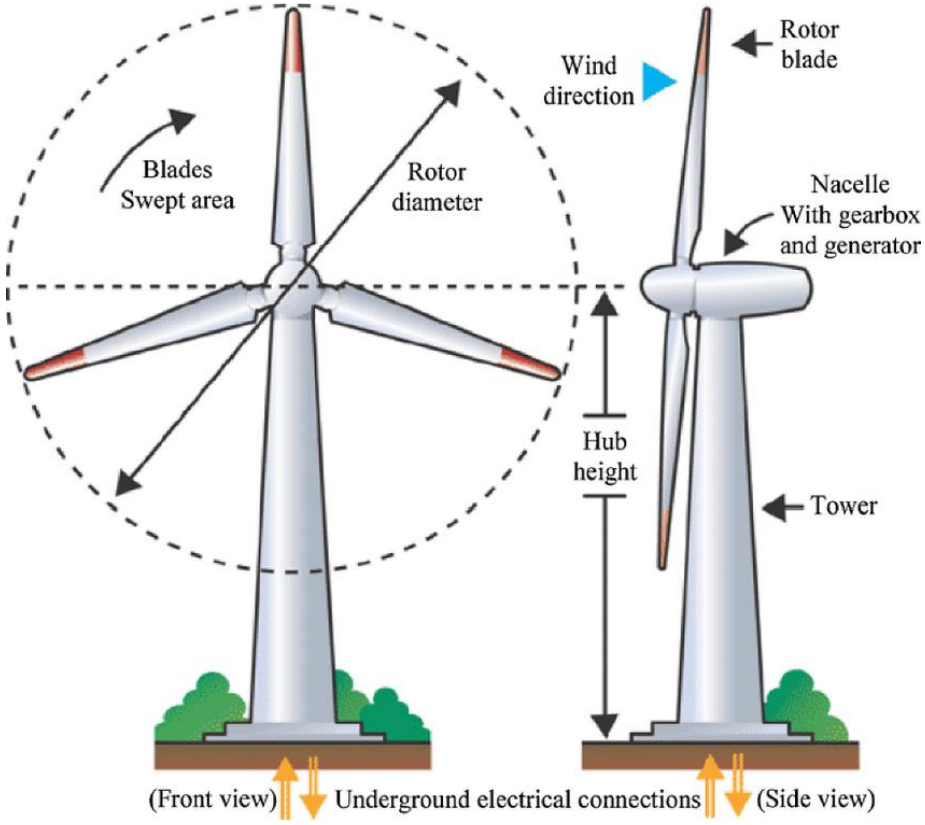

Figure 4 : Wind Turbine Schematic (Aminzadeh et al., 2023)

I.2.2. Wind Power production

To produce wind energy, a wind turbine is needed to convert the kinetic energy of moving air into mechanical energy and then into electricity through a generator. The power of the wind P_{wind} is shown by Manwell et al. (2009):

$$P_w = \frac{1}{2}\rho A v^3 \quad (1)$$

$$P_w/A = \frac{1}{2}\rho v^3 \quad (2)$$

Where P_w is the power of the moving air (in W), P_w/A is the wind power density (in W/m^2), ρ is the air density (in $kg.m^{-3}$), A the swept area of the rotors (in m^2) and v^3 the wind velocity (in $m.s^{-1}$).

The real wind power extracted by the wind turbine rotor is less than P_w . In 1919, Albert Betz established the theoretical power fraction that can be extracted from an ideal wind stream. Using the difference between upstream and downstream wind power, he estimated a limit of 59%, known as the Betz limit, of wind power which can only be converted to mechanical power (Şen, 2013). Then every wind turbine is characterised by a power coefficient Cp, which is the ratio between the wind power extracted by the turbine and the power of the wind passing through the rotors.

$$Cp = \frac{P_{extracted}}{P_w} \quad (3)$$

$$Cp_{Betz} = \frac{16}{27} \times 100 \approx 59.3\% \quad (4)$$

Where $P_{extracted}$ is the power of the wind extracted by the wind turbine, and Cp_{Betz} the Betz limit.

For an efficient and protective operation, a cut-in and cut-out wind speed is set for a wind turbine. Cut-in wind speed is the lowest wind speed at which the turbine starts energy generation, and the cut-out wind speed is the highest operational wind speed for a wind turbine. While a cut-in wind speed is designed to allow the turbine to produce sufficient energy to overcome the mechanical resistance, the cut-out wind speed allows a turbine to avoid damage from extreme wind events (Dahham et al., 2023).

I.3. Wind Resources

The wind power production is proportional to the cube of the wind speed, making wind speed a crucial factor for energy generation (Manwell et al., 2009). Then, for a wind energy project, knowledge about wind resources is essential for the turbine site selection, size

selection and cost evaluation (Duranay et al., 2024).

I.3.1. The wind speed variability

The wind speed varies from one location to another, even if they are close together. This depends mostly on local topography and the land cover. The spatial variability of wind speed in coastal and rough areas is very high (Cerralbo et al., 2015).

The wind speed also varies in time. It varies from a few seconds to a few minutes within the same area. This variability, as measured by an anemometer, gives rise to what we call turbulence and gust. While turbulence is the wind speed fluctuation around its mean value, a gust is a discrete event that occurs within a turbulence wind field. In a study of wind gust characteristics done by Hu et al. (2018), the authors explain the wind gust and its impact on wind turbine loads. The results of Zheng et al. (2022) study show that a higher turbulence intensity leads to a higher turbine blade fatigue. The temporal variability can also be on daily time scales, giving a variation in wind speed between day and night, mainly depending on the incoming solar radiation (Ashkenazy & Yizhaq, 2023). Else, for a much bigger time scale, we can distinguish seasonal, annual and interannual variation, which are driven by the climate pattern (Stuecker, 2023). Pryor et al. (2018) have shown that wind variability, especially interannual variability, directly affects the wind energy production.

Finally, wind speed varies with height and normally increases when height increases. Close to the ground, the wind is affected by the surface friction, resulting in a reduction of its speed (Bagavathsingh et al., 2016). The vertical wind profile is affected by the atmospheric stability conditions. The knowledge about whether the atmospheric conditions are neutral, stable or unstable is important because, depending on the condition, the wind gradient can be intensified or reduced. Løvøy Alvestad et al. (2024) concluded that a good understanding of the impact of atmospheric conditions on wind turbines is crucial for the turbine efficiency and energy production.

I.3.2. The wind resources Assessment

One of the direct and reliable methods used to assess the wind resources is the In-Situ Measurement-Based Estimation. It consists of the use of cup/propeller anemometers, sonic anemometers, or wind vanes for wind speed data collection. Figure 5 illustrates the different types of anemometers. Most measurements occur at ground level, typically at 10m height.

Otherwise, with the use of a weather mast, measurement can be done at a higher height (Barthelmie et al., 2016). In-situ measurement offers a high temporal resolution and is accurate at the local assessment level. However, it is cost-limited due to instruments used which are expensive and has a height constraint as the measurement height cannot align with modern wind turbine hub height which is around 100 m. Finally, those instruments are installed in discrete position then can only measure a wind speed at a specific geographic location not over an entire area (Sempreviva et al., 2008).

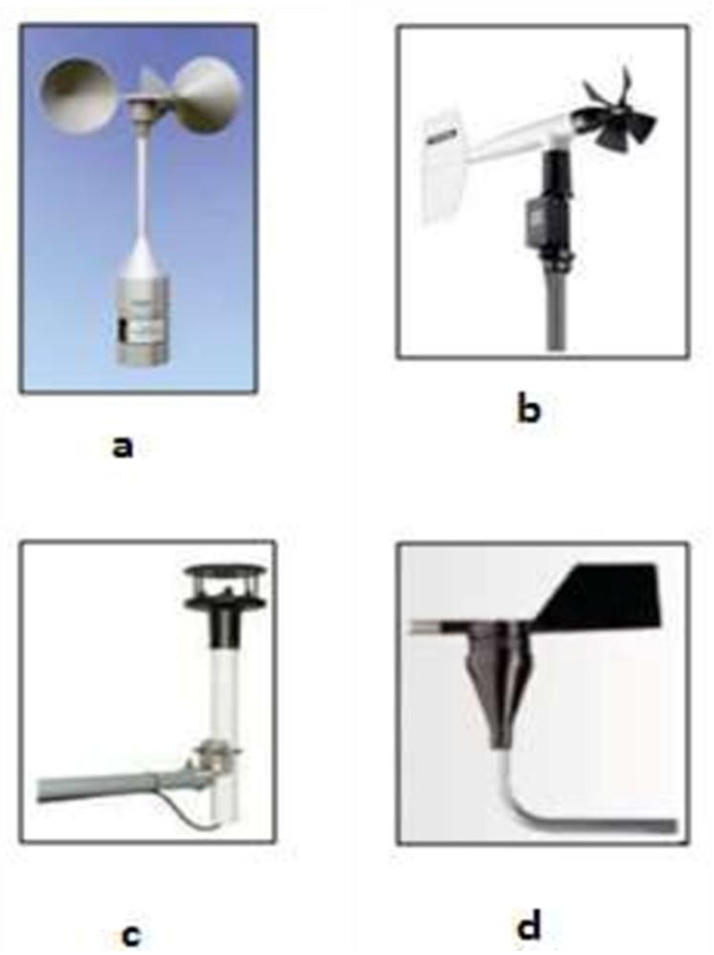

Figure 5 : a-Cup anemometer, b-Propeller Anemometer, c-Sonic anemometer, d-Wind vane (Mzough & King Ededem, 2023)

Another way to perform wind speed measurement is to use the remote sensing method. This technique is based on the Doppel Effect principle to determine the wind speed. It can be used either for onshore wind or for offshore wind using a LiDAR (Light Detection And

Ranging). Pichugina et al. (2012) described and successfully used a Doppler LiDAR system. A satellite-based sensor can also help to evaluate wind speed. Satellite data for the offshore region integrates the SAR (Synthetic Aperture Radar) Technique. It consists of observing capillary waves from the ocean surface and determining a spatial gradient (Koch & Feser, 2006).

Apart from the measurement methods, a wind resource assessment through statistical methods and numerical models is possible. The Weibull distribution is one of the statistical methods. This method is based on two main parameters: the scale parameter c and the shape parameter k (Carta et al., 2009). Many researchers use the Weibull distribution for wind resource estimation. The work of Bulut & Bingöl, (2024) concluded that the Weibull distribution is the most used statistical method between 2014 and 2023. Some other statistical methods which are also widely used are the Rayleigh distribution, derived from a fixed shape parameter of the Weibull distribution and the Gaussian distribution (Gorla et al., 2020). In terms of numerical models, we have the reanalysis dataset, the Wind Atlas, and the others simulation dataset. They are widely used for wind mapping, short-term measurement correction, bias correction and validation purposes, but always need a validation against real data (Charabi et al., 2011).

A lot of uncertainties engage in wind resource assessment. One uncertainty is a measurement error. It is related to a calibration drift and flow distortion when using instruments like anemometers and lidars during in-situ and remote sensing measurements (Klaas-Witt & Emeis, 2022). The spatial representativity of numerical model and satellite data is another uncertainty. This is due to their coarse spatial resolution. Otherwise, it is also relevant to consider the impact of climate change, which affects the climate variability and a long-term trend in wind regime. Poor quality or sparse measurement data can lead to biased wind farm models, especially when outlier data are not well detected and treated (Zou & Djokic, 2020).

I.3.3. The wind resources in Africa

Compared to Europe, where there is a rapid evolution, wind technology in Africa is still at an early stage of development. With its diversity in geography from coastal windier zones to highland plateaus, Africa has a huge wind energy potential and offers a suitable area for a large-scale wind farm. The African Renewable Energy Initiative (AREI) estimates that

Africa could generate 10GW of wind power by 2020 and over 300GW by 2030 (Pouget, 2019). Wind energy in Africa is not only abundant but also economically viable in many regions when supported by effective policies (Abbas et al., 2020). Therefore, wind energy could play a crucial role in Africa's energy mix by helping the continent shift away from fossil fuels and thereby enhance energy security (Haidi & Cheddadi, 2022). Despite its huge potential, less than 1% of Africa's electricity generation is covered by wind energy, since many African countries suffer from a lack of strong energy policy, scarcity of localised wind resources data, limited financing and international investment access, a weak grid infrastructure and transmission capacity (Agbetuyi et al., 2013).

With the use of Geographic Information System (GIS), Mentis, (2013) analysed the potential of onshore wind power on the African continent at 1 km grid resolution. The analysis shows that countries such as South Africa, Sudan, Algeria, Egypt, Libya, Nigeria, Mauritania, Tunisia, and Morocco have a high energy yield, while countries such as Equatorial Guinea, Gabon, the Central African Republic, Burundi, Liberia, Benin, and Togo have a small wind potential. In the same direction, Elsner (2019) evaluated the technical offshore wind potential over Africa. The authors found that one third of African coastal countries, including Mozambique, South Africa, Somalia, Madagascar, and Morocco, have valuable resources.

Mas'ud et al. (2017) reviewed the wind energy potential in Cameroon, Nigeria, and South Africa. The study highlights the lack of a renewable energy policy in Cameroon but concluded that the use of wind energy for electricity generation in Cameroon would be helpful in the dry season when hydro power is not available. Otherwise, the study found that the implementation of wind energy in Nigeria is slow, even if a clear policy exists. Finally, the study suggested that Cameroon and Nigeria can learn from the renewable energy progress, especially the wind's policy sector and development in South Africa.

I.4. Atmospheric Numerical Models

Emeis (2018) summarised his jobs by raising the point that it is not feasible to use direct in-situ measurement at modern wind turbine hub height. Then the remote sensing method and numerical models seem suitable for today's wind assessment. Atmospheric numerical models are tools that help to understand past observations and to provide accurate forecasting of the future Earth's climate system.

I.4.1. Overview of Atmospherics Numerical Models

Several atmospheric models exist. Here is just an overview of some of them

I.4.1.1. Reanalysis Dataset

Reanalysis is a method of combining numerical models data with past observations for the elaboration of a consistent historical dataset. This method involves the use of data assimilation to overcome observations missing data perfectly (Brönnimann et al., 2018).

ERA5 is the fifth version of the ECMWF atmospheric dataset produced in collaboration with the Copernicus Climate Change Service (C3S). A multi-height dataset spanning 137 levels from ground level to 80 km, ERA5 provides data from 1940 to the present. With 1-hour temporal resolution and 31 km spatial resolution, ERA5 use 4D-Var assimilation and is one of the most used global reanalysis datasets, but it suffers from its coarse resolution, which leads to an underestimation of peak wind events and local effects (Hersbach et al., 2020).

Another reanalysis dataset is MERRA-2, developed by the Global Modelling and Assimilation Office of NASA. MERRA-2 covers the period from 1980 to the present and uses 3D-Var assimilation. Otherwise, it offers multiple height data with a temporal resolution of 1 hour and a spatial resolution of 50km. As for ERA5, MERRA-2 also suffers from a coarse resolution (Gelaro et al., 2017). The Japan Meteorological Agency JMA produced JRA 55, a 3-hour dataset with 4D-Var assimilation. JRA55 has a spatial resolution of 55 km and a cover period from 1958 to the present time (Kobayashi et al., 2015).

The National Oceanic and Atmospheric Administration (NOAA) in collaboration with some agencies, produced 3 reanalysis datasets. The first, 20CRv3, is produced with the collaboration of CIRES and DOE. 20CRv3 is known as the longest reanalysis as it covers a period from 1836 to 2015. It has a spatial resolution of 75 km and provides 3 hours of data (Slivinski et al., 2019). The second, called NCEP-NCAR R1, is a collaboration of NCEP and NCAR. Covering a period from 1948 to the present, it has one of the coarsest resolutions, 250 km for the spatial resolution and providing 6 hours data (Hartmann, 2025). The third, call CFSR, is the first NCEP dataset, providing 1-hour data with a resolution of 38 km (Saha et al., 2010).

There are other reanalysis datasets with a good resolution. We can cite COSMO-REA6, developed by Hans-Ertel-Centre for Weather Research (HErZ) with 6 km resolution, which

can be used around Central Europe (Bollmeyer et al., 2015) and CERRA, produced by the Copernicus Climate Change Service with a resolution of 5.5 km (Ridal et al., 2024). Frank et al. (2020) and Jourdier et al. (2023) showed that CERRA and COSMO-REA6 perform better than the global reanalysis dataset. However, their field of interest is limited because they are regional reanalyses and available for a specific area.

According to Table 1 which summarises the previous reanalysis dataset, most of the global reanalysis datasets suffer from their coarse spatial resolution. However, Hartmann (2025) found that ERA5 had a better performance than MERRA-2, JRA55, NCEP-NCAR R1, NCEP-DOE R2 and NCEP/CFSv2 in a precipitation rates comparison against GPCPv2.3. Else, Foli et al. (2022) evaluated the accuracy of two reanalysis datasets, ERA5 and NCEP-NCAR reanalysis II, for the best representation of the West Africa wind regime. The results of this evaluation show that ERA5 has a better description for the wind regime of West Africa. Therefore, ERA5, with its coarse resolution, compared to other global reanalysis datasets, presents some advantages regarding its 4D-Var assimilation and the hourly data provided.

Table 1: Global Reanalysis Dataset Comparison

Dataset	**Agency**	**Period**	**Temporal resolution**	**Spatial resolution**	**Assimilation**
ERA5	ECMWF C3S	1940 to present	Hourly	31 km	4D-Var
MERRA-2	NASA	1980 to present	Hourly	50 km	3D-Var
JRA 55	JMA	1958 to present	3 Hours	55 km	4D-Var
20CRv3	NOAA (CIRES/DOE)	1836 to 2015	3 Hours	75 km	Kalman Filter
NCEP/NCAR R1	NOAA/ NCEP/ NCAR	1948 to present	6 Hours	250 km	3D-Var
CFSR	NOAA/NCEP	1979 to 2010	Hourly	38 km	3D-Var

I.4.1.2. Other Dataset

In 2000, in a big collaboration team, another NCAR-supported Numerical Atmospheric model, the Weather Research and Forecasting (WRF) model, was released. WRF is a non-hydrostatic mesoscale model widely used in many fields. It involves a 4D-var data assimilation and is very useful for weather prediction (Skamarock et al., 2008). The uses of WRF in wind resources assessment and wind energy development have been explored in several studies (Haupt & Mahoney, 2015; Liu et al., 2011; Mahoney et al., 2012)

Dynamic downscaling is a method which uses a weather model and improves the area's topographic representation with better resolved atmospheric physics and dynamics, then produces a refined dataset. Therefore, the result is a high-resolution dataset.

The German Meteorological Service (DWD) and MPI-M developed ICON (ICOsahedral Nonhydrostatic), which is a global high-resolution numerical weather model (Zängl et al., 2015). ICON comes with an icosahedral triangular grid and uses a non-hydrostatic equation. The grid that ICON has, allowed ICON to flexibly depict complex terrain surfaces such as mountainous and coastal area. ICON-LAM, a Limited-Area Mode of ICON, is a dynamical downscaled model obtained from ICON without data assimilation. This downscaling helps ICON-LAM to perform simulations at a higher spatial resolution than the original product ICON global initialized analysis. The precision of WRF, COSMO and ICON were estimated in a comparative performance study (Manco et al., 2023). The study concludes that WFR, COSMO and ICON well represented the weather conditions.

The World Bank Ground and DTU Energy developed the Global Wind Atlas (GWA), a high-resolution mapping tool. GWA provided a long-term mean wind speed and assisted in the identification of high wind potential sites. Then it is a useful tool for policymakers and specialists in sustainable energy fields (Davis et al., 2023); (Badger & Jørgensen, 2011). GWA is obtained through a dynamical downscaling process. First, from a large-scale reanalysis dataset to a mesoscale dataset with a resolution of 3 km, resulting in a generalised wind climate. Then, from the generalised wind climate to a microscale modelling system, resulting in a high 250 m resolution local wind climate (*Global Wind Atlas-Methodology*, 2023).

I.4.2. Focus on ICON-LAM, ERA5 and ERA5_GWA

A comparison of a high-resolution numerical forecast, COSMO and ICON-LAM, is done

for Romanian territory based on some surface variables, including 10 m wind speed. The study concluded that ICON-LAM performs better than COSMO (Iriza-Burcă et al., 2024). Chen et al. (2024a) ran ICON-LAM at 3.3 km spatial resolution over southern Africa for 3 years simulation from 2017 to 2019. The evaluation is based on a comparison of the simulated hourly 10 m wind speed against in-situ observation data. The study concluded that ICON-LAM in general reproduced well the observation data with a bias of 1.12 m/s.

For a study purpose over West Africa, Sterl et al. (2018) used ERA5 for an assessment of the synergies of solar photovoltaic (PV) and wind power potential, with a stability coefficient to quantify these synergies for achieving a balanced power output and limiting storage needs. The ability of ERA5 is analysed over West Africa by Gbode et al. (2023) to investigate the variability in seasonal wind resources. The authors concluded that ERA5 can assess the wind resource, but it presents bias during extreme wind events. Near-surface mean and gust wind speeds in ERA5 across Sweden are investigated by Minola et al. (2020), where the ERA5 reanalysis product has been compared to the observations in terms of wind speed and wind gust across Sweden for the period 2013–2017. The results praise ERA5 on its predecessors ERA-int (ERA interim) for wind speed and wind gust reproduction. In Ethiopia, modelling of wind power production has shown that a simulation of wind power production and the identification of wind potential areas in Ethiopia can be done using the ERA5 dataset (Nefabas et al., 2021).

A typical study comparing ICON-LAM, ERA5 and ERA5-GWA is done by Chen et al. (2024b). The authors evaluated the simulated 60 m height wind speed from the three datasets at 18 weather mast stations over South Africa. The evaluation has shown that ICON-LAM outperforms the two other datasets by underestimating the 60 m wind speed with a Mean Error (ME) of $-0.1\ m.s^{-1}$. ERA5-GWA and ERA5 underestimated the wind speed with a Mean Error (ME) $-0.3\ m.s^{-1}$ and $-1.8\ m.s^{-1}$ respectively.

I.5. The Height Scaling Methods

The atmospherics numerical dataset provides data for multiple height levels. However, to estimate the wind speed at the exact hub height for a given wind turbine, the use of height scaling methods is useful (Manwell et al., 2009).

One uncertainty introduced by the height scaling methods is the atmospheric stability. The atmospheric stability impacts the wind vertical estimation. While a neutral atmosphere led

to a predictable logarithmic wind profile, a stable and unstable atmosphere can accentuate or flatten the wind profile. Wharton and Lundquist (2012) show that the atmospheric stability consideration improves the wind assessment accuracy.

Another uncertainty is the surface roughness length. The surface roughness describes the resistance of the land surface and highly influences the frictional velocity. It is a theoretical height above the ground at which the mean wind speed would be equal to zero if the logarithmic wind profile were extrapolated downwards. It depends on the type of terrain and the land cover. Kent et al. (2017) has shown that the consideration of land cover and surface roughness length variability affects the wind speed estimation.

Typically, the use of the height scaling method, in general, is based on the power laws and the logarithmic law (Emeis & Turk, 2007).

I.5.1. The logarithmic law

The Logarithmic law is based on the theoretical and empirical research in boundary layer flows, fluid mechanics and atmospheric research (Manwell et al., 2009). It depends on the surface roughness length z_0 in meters, the Von-Karman constant k and the frictional velocity u^* in m/s. We distinguished the logarithmic linear law and the logarithmic law (Gualtieri & Secci, 2011). The logarithmic linear law is based on the Monin-Obukhov similarity theory, which implies the Monin-Obukhov stability function ψ_m and the Monin-Obukhov length L in meters:

$$V = \left(\frac{u^*}{k}\right)\left[\ln\left(\frac{z}{z_0}\right) - \psi_m\left(\frac{z}{L}\right)\right] \quad (5)$$

With V the wind speed in m/s at the height z in meters.

The logarithmic law implies a neutral stability $\psi_m = 0$:

$$V = \left(\frac{u^*}{k}\right)\left[\ln\left(\frac{z}{z_0}\right)\right] \quad (6)$$

Motta et al. (2005) used the logarithmic linear law and the logarithmic law to extrapolate 10 m wind speed to different heights up to 70 m and found an underestimation in wind speed.

I.5.2. The Power Law

The power law mostly depends on the wind power law exponent α. It also implies knowledge of the wind speed V_r at a reference height z_r.

$$V = V_r \left(\frac{z}{z_r}\right)^{\alpha} \quad (7)$$

With V the wind speed at the height z.

The power law is widely used in a lot of studies, such as (Jung & Schindler, 2021; Şen et al., 2012; Wan et al., 2019; Xu et al., 2018a).

I.5.3. The wind shear factors

The power law exponent, or more generally, the wind shear component, varies with time due to its dependence on atmospheric stability and varies with space due to its dependence on surface roughness. The extrapolation of wind speed from measurement level without atmospheric stability and terrain effect consideration could introduce significant errors (Xu et al., 2018b). The estimation of the shear component led to a different empirical formula. For a neutral atmosphere, and over a flat area, the shear component α, equal to 1/7 (0.143), is known as the one-seven law (Manwell et al., 2009).

A summary of several empirical laws for the estimation of the shear component at the international airport of Agadir Al Massira in 2016 was done by Tizgui et al. (2018). The study presented an overview of those empirical laws, and for the extrapolation of 10 m wind speed to different heights, the authors used the power law, with one shear component's empirical law to estimate the wind speed at 50 m, 80 m, and 100 m. The results show that wind speed increases with height, and above 50 m, it becomes significant.

A study of wind shear was done by Rehman and Al-Abbadi (2005). In his study, he calculated the wind shear using 20 m, 30 m and 40 m height wind speed and found a mean wind shear of 0.194 in Saudi Arabia. The mean wind shear of 0.194 allowed a higher turbine capacity factor with 6% more energy produced than the wind shear of 0.143, the typical 1/7 law shear coefficient.

The study of Crippa et al. (2021) proposed a model which captures the hourly variability of the shear component. The model of this study, which is based on Saudi Arabia, outperformed the 1/7 law.

Another study of the wind shear was also conducted by Farrugia (2003) over the Mediterranean island and the Republic of Malta using weather mast data at 10 m and 25 m.

This study revealed that wind shear component variation reaches a maximum level in January and a minimum in July.

I.6. Gap Analysis

The bibliographic review of global and regional wind energy research revealed that atmospheric numerical models are widely used in wind energy modelling and offer consistent coverage over data-scarce regions. It also shows that height scaling comes with some uncertainties, especially in areas with variable surface roughness or in complex terrain. Finally, it shows that numerous studies confirm the sensitivity of wind energy yield to wind data products, but few studies systematically compare different data sources and different scaling methods against observations at multiple heights.

In addition, there is a lack of cross-validated comparison between datasets. Most African studies use one or two types of datasets, and few compare three different types of datasets and validate their performance against in situ observation. Else, most studies use the height scaling for a particular height, and a few perform analysis through a multi-height evaluation and validation. Then, there is also a lack of multi-height study and multi-height validation within situ observation.

Therefore, this thesis is motivated by the urgent need to support the wind energy development in Southern Africa with high-resolution and validated simulation methods. It provides support to energy policy makers for selecting suitable models and reducing uncertainties in wind power simulation.

Conclusion

The Above chapter highlights the importance of this study. With the deep review of the literature and the main studies on atmospheric dataset and height scaling methods, it shows the direction of analysis of this study, based on the existing lack. The next chapter will present the methodology followed by this study.

CHAPTER II: MATERIALS AND METHODS

CHAPTER II: MATERIALS AND METHODS

Introduction

This chapter starts with the presentation of the study area through a map with the geographic location of all stations. It is followed by a description of the three datasets involved in this study, and the chapter ends with tools and methodology.

II.1. Study Area and Study Periods

Due to data availability, this analysis was over 3 years starting from January 2017 to December 2019 and the study area is the Southern part of Africa. According to the Global Wind Atlas, this region has a good wind potential suitable for wind energy generation (Davis et al., 2023). Stations involved in this study are located from 16°S to 38°S, and 9°E to 39°E.

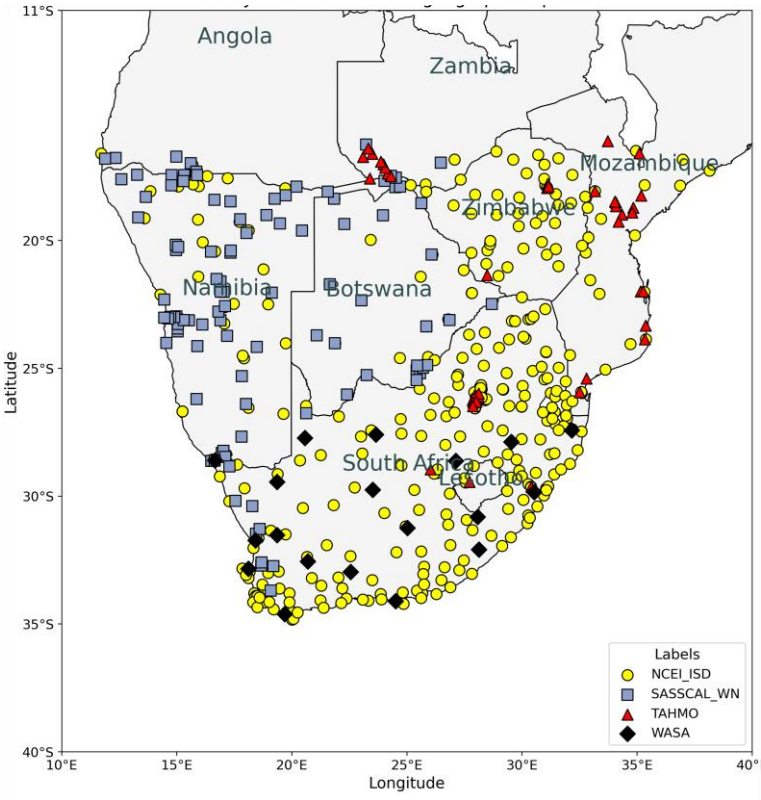

Figure 6: Map of the Study

Four labels, TAHMO, NCEI_ISD, SASSCAL_WN and WASA, with a total of 493 sites involved in the study. The 493 sites are meteorological network stations and weather mast stations. All of them are identified by their geographic coordinates and names or codes.

Figure 6 presented the map of the study area where the yellow circles represent the NCEI_ISD stations, the sky-blue squares represent the SASSCAL_WN stations, the red triangles represent TAHMO stations and black diamond-shaped markers represent WASA stations .All information about those four labels is detailed in the next part.

II.2. Datasets

II.2.1. Observed Datasets

The observation data involved in the study are in-situ measurements coming from weather mast stations, in-situ data coming from local meteorological stations, and the surface integrated database.

Eighteen weather mast stations from Wind Atlas for South Africa (WASA) are involved in this study (Wind Atlas for South Africa, 2010). They form what is called label WASA in this study. Hourly wind speed data, over the study period, at four (04) different heights, 10 m, 20 m, 40 m, and 60 m, were downloaded. Those mast stations are named from WM01 to WM19, except WM04, which has no data. Otherwise, some stations did not provide full data over the entire 3-year time stamps of the study. The temporal data coverages of each weather mast wind speed at different heights are shown by a pie chart in Figure 7. The white colour is the percentage of missing data from 2017 to 2019 for a specific mast station.

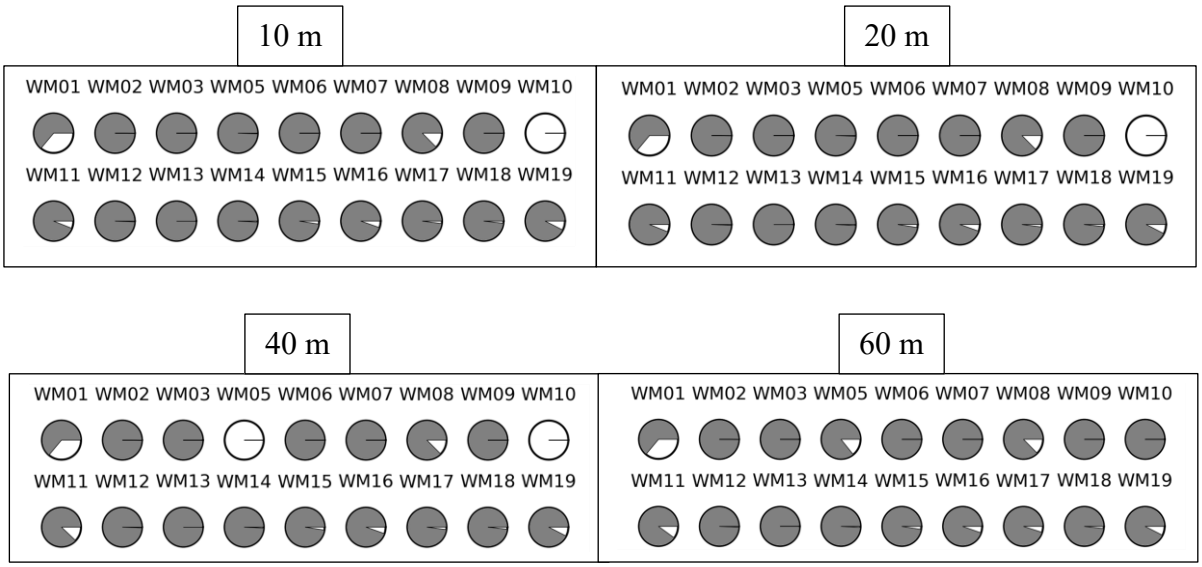

Figure 7: Pie Chart of weather mast temporal data coverage

The local meteorological station's data are from two services. The first service is the Trans-

African Hydro-Meteorological Observatory, which develops a hydro-meteorological station network in sub-Saharan Africa. Those stations are labelled as TAHMO in this study. The second is the Southern African Science Service Centre for Climate Change and Adaptive Land Management (SASSCAL), which is an initiative within Southern Africa, such as Angola, Botswana, Namibia, South Africa, and Zambia, with funding from Germany. SASSCAL developed a meteorological station network called SASSCAL Weather Net, which is labelled here as (SASSCAL_WN). The last observation data is a global hourly Integrated Surface Database (ISD) collected from several sources through the National Center for Environmental Information (NCEI). Data from NCEI in this study are labelled (NCEI_ISD).

42 stations from the label TAHMO, 104 stations from the label SASSCAL_WN and 329 stations from the label NCEI are investigated for evaluating simulated 10 m wind speed. All these data are open-source data and can be easily accessed through their original website.

II.2.2. Simulated Datasets

Three (03) simulated datasets are used in the study. The dynamical downscaled dataset ICON-LAM, the reanalysis ERA5 dataset and the statistical downscaling variant of ERA5 (ERA5_GWA).

The ICON-LAM dataset used is a regional setup of the ICON atmospheric model (Zängl et al., 2015). It has a spatial resolution of 3.3 km. The setup and configuration details are provided by Chen et al. (2024a). While ICON-LAM data from TAHMO, SASSCAL_WN and NCEI_ISD are hourly resolution data, the WASA data are on 15-min bases, then are averaged on hourly resolution.

The ERA5 reanalysis data is produced by ECMWF with 31 km spatial and 1-hour temporal resolution. ECMWF provided eastward and northward (u, v) components wind speed and the horizontal wind speed is obtained by computing the square root of the sum of u^2 and v^2 wind speed (Hersbach et al., 2020).

The ERA5_GWA is a statistical downscaled product of a combination of ERA5 and GWA. It is obtained by multiplying the time series of ERA5 by the ratio between the long-term mean wind speed of GWA and ERA5. As a result, ERA5_GWA has a spatial resolution of 250 m. This is shown by the equation (8)

$$ERA5\_GWA = ERA5_{time\ series} \times \frac{GWA_{Long-term\ mean}}{ERA5_{Long-term\ mean}} \quad (8)$$

Several studies use this statistical downscaling approach to combine the reanalysis dataset with GWA from the perspective of obtaining a high-resolution dataset. While Gruber et al. (2021) and Murcia et al. (2022) combine ERA5 with GWA for a renewable energy potential study, González-Aparicio et al. (2017) and Ryberg et al. (2019a) apply the same approach to MERRA-2.

II.3. Methods and tools

II.3.1. Preprocessing

The analysis started with a preprocessing which only concerns the observed data and the ICON-LAM dataset. It involved a data cleaning process and a process to fix a time zone to UTC.

The data cleaning on ICON-LAM is basically to remove duplicate station data in case of multi-station data on one ICON grid, and to remove stations where all values are the same over the study time. For the observed data, data cleaning was used to remove implausible data. According to the Beaufort wind scale table, at 10 m height on a flat area, the wind speed of 32.7 (m/s) and above is considered hurricane wind (World Meteorological Organization, 2019). Therefore, in this study, the wind speed at 10 m height on a flat area of 40 (m/s) and above is considered implausible data and is removed from the database. We also fix a threshold of 70% and then remove all stations with more than 70% missing values. This threshold was also applied by Chen et al. (2024a). At the end, 204 (78 from SASSCAL_WN, 24 from TAHMO and 102 from NCEI_ISD) stations' data and 18 weather mast station data remain for the study.

II.3.2. Metrics

Four metrics are used in this study. The Mean Absolute Error (MAE), the Mean Error (ME), the Pearson correlation coefficient (Pearson r), and Perkins Skill Scores (PSS). Let assume O_i data from observation, $\overline{O}$ the average of observed data, X_i data from a simulated dataset, $\overline{X}$ the average of simulated data, F_X the frequency distribution of simulated data, F_O the

frequency distribution of the observation data, n the total number of data and b the number of bins for the frequencies estimation.

II.3.2.1. The Mean Absolute Error (MAE)

MAE is obtained by the average of the absolute differences between the simulation product and the Observation. It gives the average magnitude of the errors without direction consideration. A lower value of MAE means satisfactory performance of the simulated dataset. The mathematical formula is:

$$MAE = \frac{1}{n}\sum_{i=1}^{n} |X_i - O_i| \tag{9}$$

II.3.2.2. The Mean Error (ME)

ME is obtained by the average differences between the simulation product and the Observation. It gives the average magnitude of the errors with direction consideration, indicating an over- or underestimation of the simulated product. Then a positive ME means an overestimation of the observation and a negative ME, an underestimation. Otherwise, a value of ME close to zero (0) means satisfactory performance of the simulated dataset. The mathematical formula is:

$$ME = \frac{1}{n}\sum_{i=0}^{n} X_i - O_i \tag{10}$$

II.3.2.3. The Pearson correlation coefficient (Pearson r)

Pearson r evaluates the linear relationship between the observations and the simulated data. In the range of [-1; 1], -1 indicates a negative correlation and 1 indicates a positive correlation. The mathematical formula is:

$$r = \frac{\sum_{i=0}^{n}\left(X_i - \overline{X}\right)\left(O_i - \overline{O}\right)}{\sqrt{\sum_{i=0}^{n}\left(X_i - \overline{X}\right)^2}\sqrt{\sum_{i=0}^{n}\left(O_i - \overline{O}\right)^2}} \tag{11}$$

II.3.2.4. The Perkins Skill Score (PSS)

PSS analyses the frequency distribution of the simulation and the observation and then estimates their overlapping area (Perkins et al., 2007). In the range [0; 1], PSS equal to 1 indicates a perfect overlap, which represent an outstanding performance and PSS equal to 0 means the worst performance. The mathematical formula is:

$$PSS = \sum_{1}^{b} \min(F_X; F_O) \tag{12}$$

II.3.3. The Taylor Diagram

The Taylor diagram is a polar diagram in a 2-D plot, which shows the correspondence between simulated and observed values, using statistical metrics. It is a powerful plot presenting jointly the correlation, the standard deviation, and the root mean square error. It is a useful tool for complex models, with multiple variables and multiple dimensions, such as a geophysical model, for evaluation and comparison. It also allows us to define skill scores for the model classification (Taylor, 2001). The mathematical formula of the Taylor skill scores is:

$$S = \frac{4(1+r)^4}{\left(\frac{\sigma_x}{\sigma_o} + \frac{\sigma_o}{\sigma_x}\right)^2 (1+r_0)^4} \tag{13}$$

Where r is the correlation coefficient of the simulation, r_0 the maximum correlation attainable (here $r_0 \approx 1$), σ_x the standard deviation of the simulation and σ_o the observation standard deviation. The use of the Taylor Diagram for model validation is common in atmospheric model studies (Coppola et al., 2024; dos Santos Silva et al., 2023).

The methodology employed in this study involves the utilisation of the Taylor skill score S to establish a ranking of all methods, based on the average value over all the 18 weather mast stations of the corresponding metrics (standards deviation, Pearson correlation, and the root mean square error).

II.3.4. The Different Height Scaling Methods

To scale a wind speed to a specific height called the target height, we need the knowledge of the wind speed at a certain height called the reference height. In this study, we call the Advanced method a height scaling method, which involves the use of reference heights wind speed available from the vertical levels of numerical atmospheric data sets remarkably close to the target height. In total, ten (10) different methods were used in this study.

II.3.4.1. The Linear Interpolation

For this method, the knowledge of wind speed $\boldsymbol{V_1}$ and $\boldsymbol{V_2}$ at the two nearest reference heights $\boldsymbol{z_1}$ and $\boldsymbol{z_2}$, at the target height $\boldsymbol{z}$ are used. In this study, the linear interpolation

method is called Advanced Linear Interpolation (**Adv_Lin**). To estimate the wind speed V_z at the target height, we use the formula:

$$\boldsymbol{Adv\_Lin}: \quad \boldsymbol{V_z = V_1 + \left(\frac{z - z_1}{z_2 - z_1}\right)(V_2 - V_1)} \tag{14}$$

II.3.4.2. The Logarithmic Law

The logarithmic law in this study assumes the Monin-Obukhov stability function equals zero ($\psi_m = 0$). To estimate the wind speed $\boldsymbol{V_z}$ at the target height $\boldsymbol{z}$, the following formula is used:

$$\boldsymbol{V_z = V_1 \frac{ln\frac{(z-d)}{z_0}}{ln\frac{(z_1-d)}{z_0}}} \tag{15}$$

With $\boldsymbol{z_0}$ the surface roughness length, $\boldsymbol{d}$ the displacement height (in this case $\boldsymbol{d = 0}$) and $\boldsymbol{V_1}$ the wind speed at the reference height $\boldsymbol{z_1}$. In the analysis, we make the uses of the Logarithmic law in two ways. One with the knowledge of the nearest reference height wind speed, which is called the advanced logarithmic law (**Adv_Log**), and the second is any target height (in this case, 10 m height), which is called the simple logarithmic law (**LogLaw**).

II.3.4.3. The Power Law

The use of the power law is driven by the estimation of the wind power law exponent. One method to estimate the wind power law exponent in this study is the so-called Advanced Power law method (**Adv_Pl**), which involves the knowledge of the wind speed $\boldsymbol{V_1}$ and $\boldsymbol{V_2}$ at the two nearest heights $\boldsymbol{z_1}$ and $\boldsymbol{z_2}$ to the target height (Devis et al., 2018). The power law exponent is then estimated by:

$$\boldsymbol{\alpha = \frac{\ln(V_1/V_2)}{ln(z_1/z_2)}} \tag{16}$$

Another way is the use of empirical laws, which estimate the wind shear from some specific criterion, such as the land topography, the surface roughness, and weather conditions. The validity of empirical Laws is limited to the lower atmosphere up to 200 m above the ground level (Tizgui et al., 2018). Table 2 summarises all the empirical methods used in this study.

The most used empirical law is the well-known one-seven law (hereafter **1_7_Law**). The wind shear is estimated for a neutral atmosphere to 1/7= 1.143 (Manwell et al., 2009).
Another expression for the wind shear is proposed by Counihan, (1975). The expression depends only on the surface roughness length (hereafter **Counihan_Law**). It suggests that, for the surface roughness length between 0.001m and 10 m ($0.001m < z0 < 10\text{m}$), the shear component is expressed by:

$$\alpha = 0.096 \log_{10} z_0 + 0.016(\log_{10} z_0)^2 + 0.24 \quad (17)$$

Spera, (1994) used an expression proposed by NASA researchers. The equation (**Spera_Law**) is based on the surface roughness and the wind speed at the reference height.

$$\alpha = \left(\frac{z0}{h1}\right)^{0.2} (1 - 0.55 \log(V_1)) \quad (18)$$

Another equation (hereafter **Justus_Law**) is proposed by Justus C., relying only on the wind speed at a reference height of 10m (Justus & Mikhail, 1976).

$$\alpha = \frac{0.37 - 0.088 \ln(V_1)}{1 - 0.088 \ln\left(\frac{z_1}{10}\right)} \quad (19)$$

Khalfa et al. (2014) proposed an expression (**Khalfa_Law**), which takes into consideration the stability conditions and the geographic mean height.

$$\alpha = \frac{1}{\ln\left(\frac{z_g}{z_0}\right)} - \frac{0.0881}{1 - 0.0881 \ln\left(\frac{V_1}{z_0}\right)} \ln\left(\frac{V_1}{V_n}\right) \quad (20)$$

The last empirical law (hereafter **Nfaoui_Law**) investigated in this study is proposed by Nfaoui et al. (1998) through the formula:

$$\alpha = \frac{x - 0.0881 \ln(V_1)}{1 - 0.0881 \ln\left(\frac{z_1}{10}\right)} \quad (21)$$

where $x = 0.25$ for $z_0 \in [0.000m; 0.005m]$, $x = 0.31$ for $z_0 \in [0.005m; 0.050m]$, $x = 0.27$ for $z_0 \in [0.050m; 0.500m]$ and $x = 0.48$ for $z_0 \in [0.500m; 4.000m]$

Table 2 : List of Empirical Law

Methods	Empirical Formula	References
1_7_Law	$\alpha = 1.143$	(Manwell et al., 2009)
Counihan _Law	$\alpha = 0.096 \log_{10} z_0 + 0.016(\log_{10} z_0)^2 + 0.24$	(Counihan, 1975)
Justus_Law	$\alpha = \frac{0.37 - 0.088 \ln(V_1)}{1 - 0.088 \ln\left(\frac{z_1}{10}\right)}$	(Justus & Mikhail, 1976)
Spera_Law	$\alpha = \left(\frac{z0}{h1}\right)^{0.2} (1 - 0.55 \log(V_1))$	(Spera, 1994)
Khalfa_Law	$\alpha = \frac{1}{\ln\left(\frac{z_g}{z_0}\right)} - \frac{0.0881}{1 - 0.0881 \ln\left(\frac{V_1}{z_0}\right)} \ln\left(\frac{V_1}{V_n}\right)$	(Khalfa et al., 2014)
Nfaoui_Law	$\alpha = \frac{x - 0.0881 \ln(V_1)}{1 - 0.0881 \ln\left(\frac{z_1}{10}\right)}$	(Nfaoui et al., 1998)

II.3.5. The Surface Roughness length and the Wind Energy estimation

The European Space Agency Climate Change Initiative (ESA CCI) includes a Land Cover project whose aim is to generate a global land cover product. This consists of a generation of a tool which provides for a specific geographic area, a land cover types and a land cover code (Chirachawala et al., 2020). The Renewable Energy Simulation toolkit (RESKit) is a powerful tool for the large-scale simulation of renewable energy systems (Ryberg et al., 2019; https://github.com/FZJ-IEK3-VSA/RESKit). RESKit provides a table which links ESA CCI land cover code to a corresponding surface roughness length. The use of height scaling methods to scale 10m wind speed to different heights implies the knowledge of the surface roughness length. In this study, ESA CCI Land cover is used to provide a Land cover code for the 18 specific weather mast stations. Otherwise, the RESKit table is used to assign the specific surface roughness length to every weather mast station.

The wind energy is estimated over the 3-years study time periods from 2017 to 2019. The wind energy density estimation is done with the formula:

$$E/A = \frac{1}{2}\rho \sum_{i=1}^{N} U_i^3$$

Where E/A is the energy density in Wh/m², U_i the hourly wind speed in m/s, N the number of wind speed measurement in the 3 years study period in hourly bases and ρ the air density in kg/m³ (Manwell et al., 2009). For the evaluation, a boxplot of the Relative Deviation (RD) in percentage of the energy density is used.

$$RD = \frac{E/A_x - E/A_{obs}}{E/A_{obs}} \times 100$$

Where the E/A_x is the energy density for the simulated product in Wh/m² and E/A_{obs} the energy density of the observation in Wh/m².

Conclusion

This chapiter provided a comprehensive overview of the study area and study period of the research. The geographical locations of all stations affiliated with the TAHMO, NCEI_ISD, SASSCAL_WN and WASA labels have been well presented. A details account of the observed data, as well as the three atmospheric datasets ICON-LAM, ERA5 and ERA5_GWA provided a deep understanding of the characteristics and the relevance of each product. Furthermore, the metrics, analytical and statistical tools involve in this study have been explained. This assured a good understanding of the analysis and the founding, which will be part of the next chapter.

CHAPTER III: RESULTS AND DISCUSSIONS

CHAPTER III: RESULTS AND DISCUSSION

Introduction

This chapter highlights all results of this study. It starts with the comparison of simulated 10 m wind speed over 204 stations across the southern Africa using the MAE, ME, Pearson r, and PSS. The next part of this chapter is the evaluation of height scaling methods and dataset throughout a boxplot and Taylor diagram. Then finally the chapter will end with the wind energy estimation.

III.1. Datasets Comparison at 10m

Simulated 10 m wind speed data from the three datasets ICON-LAM, ERA5 and ERA5_GWA are compared against observation data over 204 stations of labels TAHMO, SASSCAL_WN and NCEI_ISD. For this comparison, four metrics are used, and for every metric, a scatter plot and box plot will help for results visualisation (Figure 8, Figure 9, Figure 10, Figure 11, Figure 12, Figure 13, Figure 14, and Figure 15). In the scatter plot, the different stations are represented according to their labels shape markers (square for SASSCAL_WN, triangle for TAHMO and circle for NCEI_ISD) and to the colour of their metric values. For the boxplot, the first 3 boxes show the variation across the labels (green for SASSCAL_WN, grey for TAHMO, and blue for NCEI_ISD) and the last box in pink is for all stations together. The yellow markers show the dispersion of stations across every label, and the number of stations of every label is written above every box.

III.1.1. MAE

In general, few stations have a higher MAE than 3.0 m/s. ERA5_GWA outperforms the other datasets in terms of MAE with an average over all stations of 1.33 m/s, followed by ERA5 with an average of 1.50 m/s and then ICON-LAM with 1.77 m/s has a lower performance. Table 3 provides a summary of the statistics of the MAE comparison

Table 3: Statistic of MAE comparison at 10 m

Datasets	1st Quartiles	2nd Quartiles	3rd Quartiles	90% of stations
ERA5_GWA	0.97	1.15	1.46	1.93
ERA5	1.14	1.32	1.67	2.22
ICON-LAM	1.44	1.64	2.00	2.47

It shows the MAE statistics (in m/s) for the three quartiles, and for 90% of stations confirming the good performance of ERA5_GWA in terms of MAE. Figure 8 displays the MAE results through a scatter plot, and Figure 9 displays it through a boxplot.

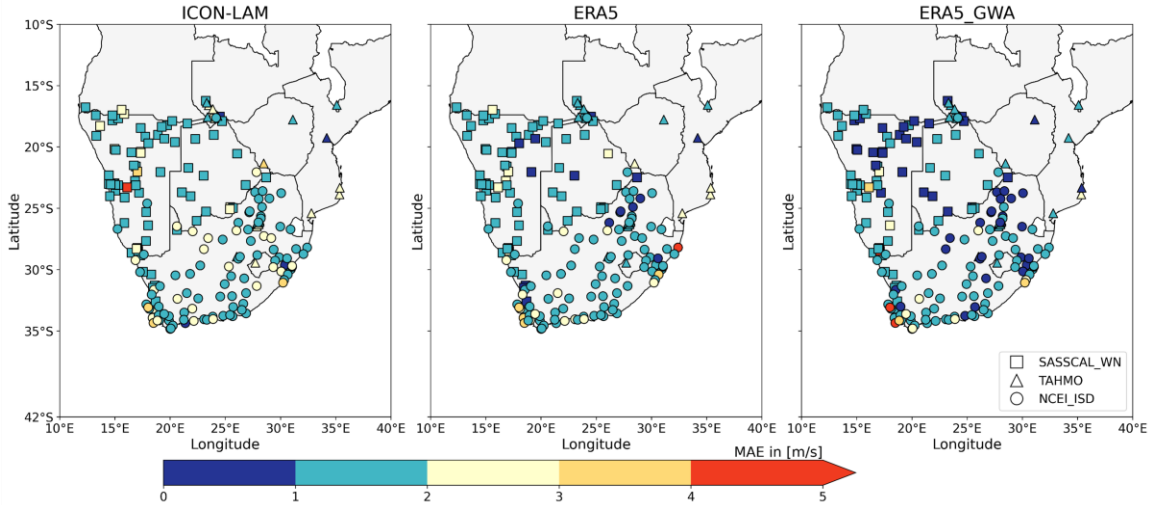

Figure 8: Scatter plot of MAE comparison of Datasets vs Observation at 10m

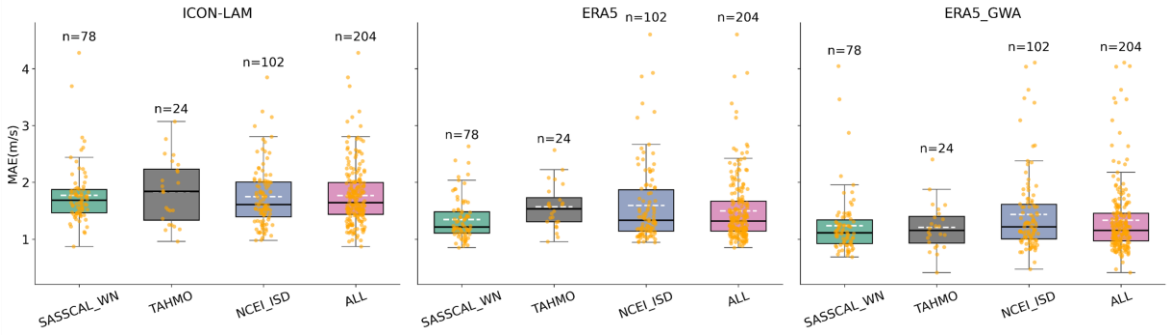

Figure 9: Box plot of MAE comparison of Datasets vs Observation at 10m

Finally, the MAE results of specific station are summarised by **Table** 4

Table 4: MAE results for specific stations

Datasets	**Lowest bias**			**Highest Bias**		
	MAE	**Station**	**Location**	**MAE**	**Station**	**Location**
ERA5_GWA	0.41	TA00546	17.78°S 31.13°W	4.11	68815099999	33.08°S 18.02°W
ERA5	0.85	67593	22.49°S 28.70°W	4.60	68491099999	28.20°S 32.42°W
ICON-LAM	0.87	65934	17.55°S 24.53°W	4.28	103	23.30°S 16.12°W

III.1.2. ME

Globally, ERA5_GWA outperforms ERA5 and ICON-LAM in terms of ME with an error value of +0.39 m/s, +0.75 m/s, and +1.23 m/s, respectively. ICON-LAM tends to overestimate the 10 m wind speed, with 95.10% of overestimation stations and only 4.90% of underestimation stations, while ERA5_GWA recorded 32.84% of underestimation stations and 67.16% of overestimation stations. Figure 10 and Figure 11, which present respectively the scatter plot and the box plot of ME comparison, confirm the tendency of each dataset. A summary of the statistics of the ME comparison is provided by Table 5, and Table 6 present the results of some specific stations.

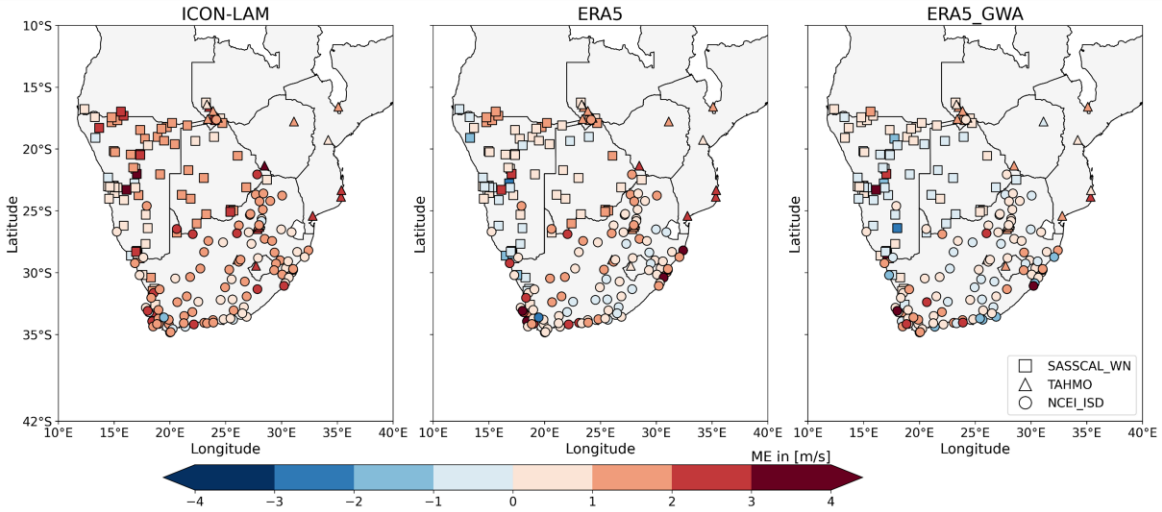

Figure 10: Scatter plot of ME comparison of Datasets vs Observation at 10m

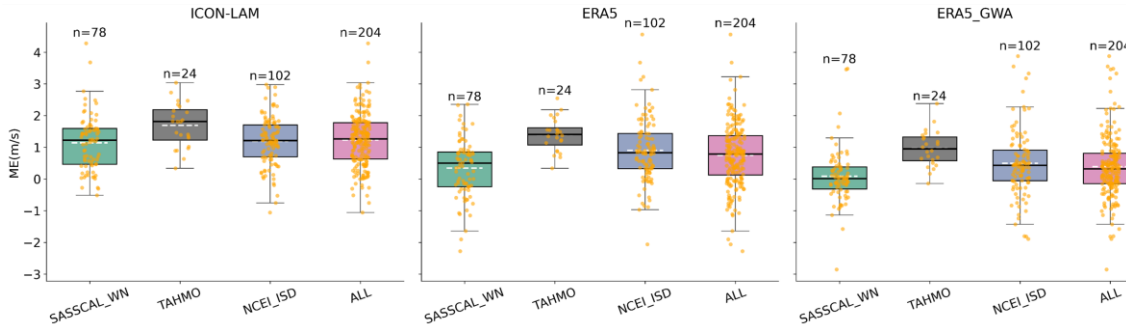

Figure 11: Box plot of ME comparison of Datasets vs Observation at 10m

Table 5: Statistic of ME comparison at 10 m

Datasets	1st Quartiles	2nd Quartiles	3rd Quartiles	90% of stations
ERA5_GWA	-0.14	0.32	0.81	1.47
ERA5	0.13	0.79	1.37	1.97
ICON-LAM	0.63	1.26	1.77	2.29

Table 6: ME results for specific stations

Datasets	Lowest error			Highest error		
	ME	Station	Location	ME	Station	Location
ERA5_GWA	-2.85	31196	26.40°S 18.01°W	+3.88	68815099999	33.08°S 18.02°W
ERA5	-2.27	31210	22.79°S 16.81°W	+4.57	68491099999	28.20°S 32.42°W
ICON-LAM	-1.05	68821099999	33.62°S 19.47°W	+4.28	103	23.30°S 16.12°W

III.1.3. Pearson r

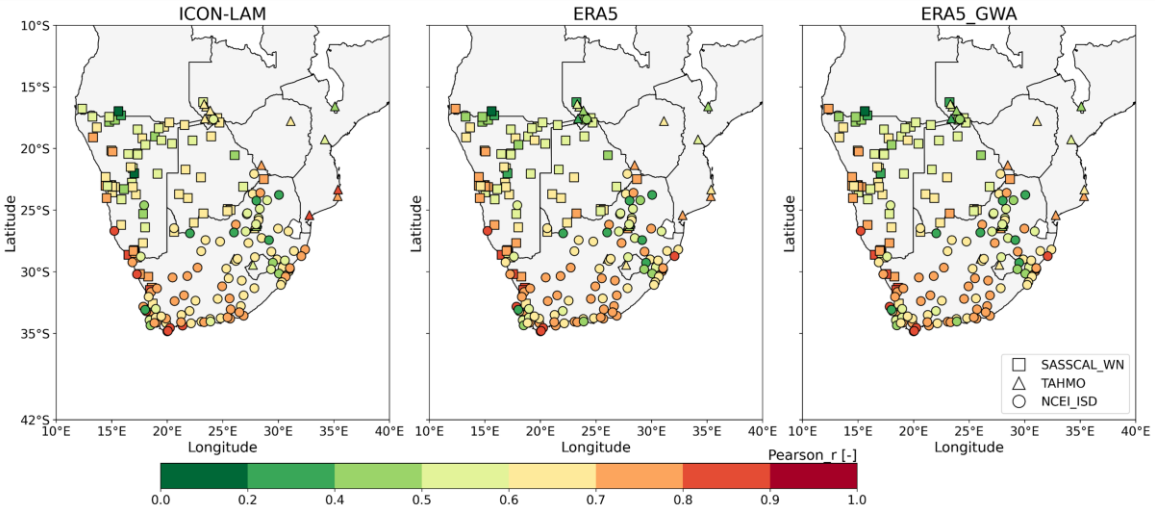

Figure 12: Scatter plot of Pearson r comparison of Datasets vs Observation at 10m

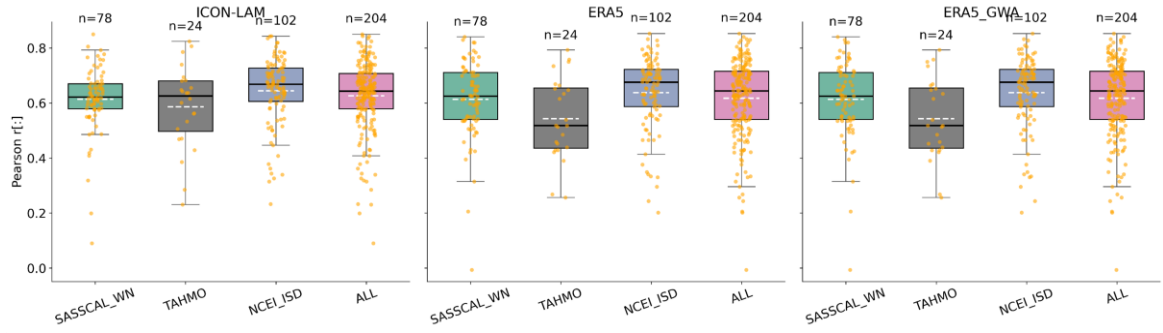

Figure 13: Boxplot of Pearson r comparison of Datasets vs Observation at 10m

ERA5_GWA is obtained from a statistical downscaling of ERA5. This statistical downscaling affects the magnitude but not the correlation. Then, ERA5_GWA is obtained

with a different magnitude compared to ERA5, but it strictly has the same correlation coefficient. Therefore, ERA5_GWA and ERA5 recorded the same correlation for every station. In general, the three datasets have similar correlation coefficients, with a slight advantage for ICON-LAM, which has an average correlation coefficient over all stations of 0.626, while ERA5 and ERA5_GWA have a coefficient of 0.617. Figure 12 shows the Pearson r result with a scatter plot, but due to the similar performance of the three datasets, it is difficult to find any trend. Using Figure 13, which presents the results of Pearson r with a box plot, and **Table *7***, which summarises the results by quartiles, the slight advantage of ICON-LAM can be identified. **Table *8*** presents the results of Pearson r for some specific stations.

Table 7: Statistic of Pearson r comparison at 10 m

Datasets	1st Quartiles	2nd Quartiles	3rd Quartiles	90% of stations
ICON-LAM	0.580	0.643	0.707	0.769
ERA5_GWA & ERA5	0.540	0.643	0.715	0.769

Table 8: Pearson r results for specific stations

Datasets	Lowest correlation			Highest correlation		
	Pearson r	**Station**	**Location**	**Pearson r**	**Station**	**Location**
ICON-LAM	0.090	46943	16.98°S 15.62°W	0.850	858577	28.63°S 16.51°W
ERA5_GWA & ERA5	0.000	46943	16.98°S 15.62°W	0.853	68926399999	34.56°S 20.25°W

III.1.4. PSS

As for Pearson r, the three datasets have similar performance in terms of PSS. Table 9 summarises the statistics of the PSS comparison and then shows the similarity between dataset's performance across different quartiles for the PSS comparison.

Table 9: Statistic of PSS comparison at 10 m

Datasets	1st Quartiles	2nd Quartiles	3rd Quartiles	90% of stations
ERA5_GWA	0.652	0.755	0.827	0.892
ICON-LAM	0.605	0.735	0.815	0.887
ERA5	0.597	0.722	0.812	0.875

Figure 14 presents the PSS results with a scatter plot and Figure 15 presents the same results with a boxplot.

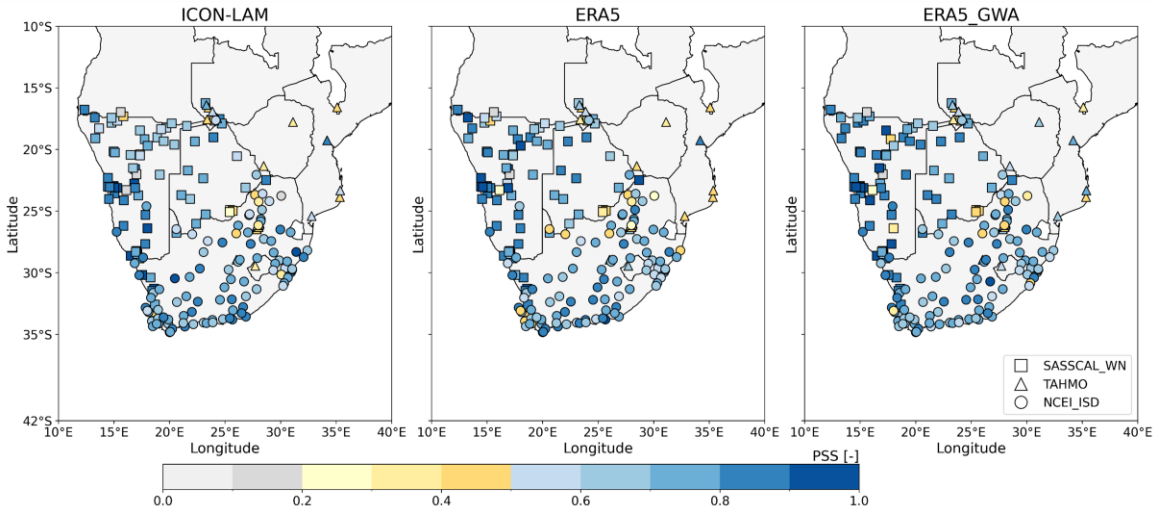

Figure 14: Scatter plot of PSS comparison of Datasets vs Observation at 10m

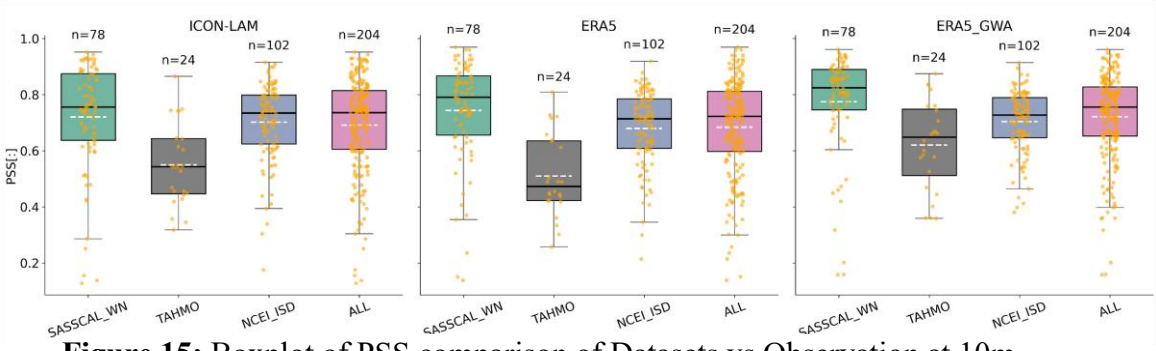

Figure 15: Boxplot of PSS comparison of Datasets vs Observation at 10m

Table 10: PSS results for specific stations

Datasets	**Lowest score**			**Highest score**		
	PSS	**Station**	**Location**	**PSS**	**Station**	**Location**
ERA5_GWA	0.158	46943	16.98°S 15.62°W	0.960	E7625	23.44°S 15.05°W
ERA5	0.138	46943	16.98°S 15.62°W	0.969	114	19.71°S 18.04°W
ICON-LAM	0.128	46943	16.98°S 15.62°W	0.951	E7626	23.10°S 15.03°W

Table 10 provides the results of some specific stations. In general, with a slight advantage, ERA5_GWA performs well in terms of PSS with an average over all stations value of 0.721, followed by ICON-LAM with an average of 0.691 and then ERA5_GWA with an average of 0.684.

III.2. Height scaling methods evaluation

The height scaling methods analysis is done through two evaluations. The evaluation of the observed 10m wind speed scaled to different heights and the simulated 10 m wind speed scaled to different heights. For the metrics calculation, a cut-in and cut-out wind speed of respectively 2.0 m/s and 25 m/s is set on the observed wind speed.

III.2.1. Evaluation of the Observed 10m scaled to different heights

The 10 m wind speed from WASA at the 18 weather mast stations are scaled to 20 m, 40 m, and 60 m throughout seven scaling methods: 1_7_Law, Counihan_Law, Justus_Law, Khalfa_Law, Nfaoui_Law, and Spera_Law. This analysis highlights the effective impact of different scaling methods on the wind speed without any dataset influence because the scaling was done using the observed data itself.

In general, the performance of the different methods decreases with an increase in scaling heights and the dispersion across stations increases with an increase in scaling height. Then, the scaling from 10 m to 60 m introduced the highest errors, followed by the scaling from 10 m to 40 m and the lowest errors were recorded for a scaling from 10 m to 20 m. Otherwise, the performance of all methods follows the same trend for every scaling (10 m to 20 m, 10 m to 40 m, and 10 m to 60m). However, the performance variation across the different methods is more remarkable for a scaling from 10 m to 60 m. Therefore, the discussion will focus on the scaling from 10 m to 60 m. For every metric, a box plot is used for the results presentation. The results presentation will focus on the third quartile (the results of 75% of stations).

The results of all methods are summarised in Table 15 (see the appendices)

III.2.1.1. MAE

Globally, it is evident that the 1_7_Law and Counihan_Law, characterised by low dispersion across different stations, demonstrate superior performance with a low bias of respectively 1.15 m/s and 1.13 m/s. Conversely, the Justus_Law followed by Khalfa_Law, distinguished by high dispersion and median, demonstrate low performance due to high bias of 1.44 m/s and 1.31 m/s, respectively. Nfaoui_Law, LogLaw and Spera_Law demonstrate commendable performance, as evidenced by their low median values. However, it is noteworthy that these laws exhibit a considerable degree of dispersion across different stations in comparison to Counihan_Law and 1_7_Law. Figure 16 presents the MAE results for the scaling methods comparison.

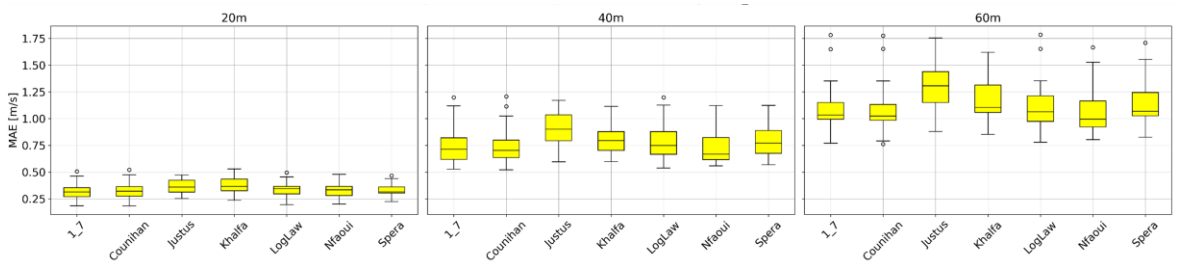

Figure 16: Boxplot of MAE comparison of scaling methods at multiple heights

III.2.1.2. ME

Figure 17 presents the ME results for the scaling methods comparison. The results show that the 1_7_Law and Counihan_Law tend to underestimate the scaled wind speed, while Justus_Law and Spera_Law tend to overestimate it. Khalfa_Law, Nfaoui_Law, and LogLaw demonstrate a good performance with a slight overestimation.

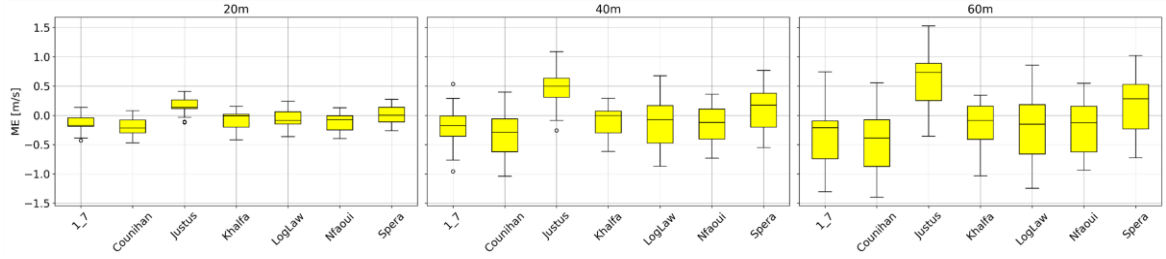

Figure 17: Boxplot of ME comparison of scaling methods at multiple heights

III.2.1.3. Pearson r

All the methods have an almost perfect Pearson correlation. They all have similar correlations, and the differences between them are negligible. For a scaling of 10 m to 20 m, all have a Pearson correlation of 0.995, a Pearson correlation of 0.98 for a scaling from 10 m to 40 m and then a Pearson correlation of 0.95 for a scaling from 10 m to 60 m. Figure 18 presents the Pearson correlation results for the scaling methods comparison

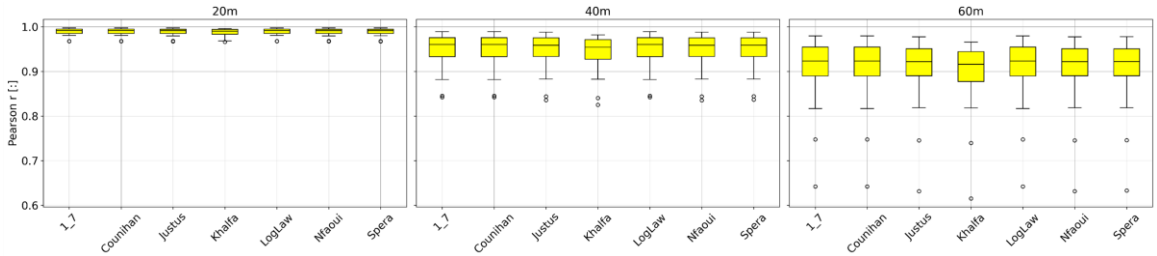

Figure 18: Boxplot of Pearson r comparison of scaling methods at multiple heights

III.2.1.4. PSS

In general, all methods have good Perkins Skill Scores, which are above 0.80. Counihan_Law, 1_7_Law, and LogLaw exhibit similar and the highest score of 0.94, 0.92, and 0.90, respectively, while Khalfa_Law demonstrates the lowest score of 0.86. Figure 19 presents the PSS results for scaling methods comparison.

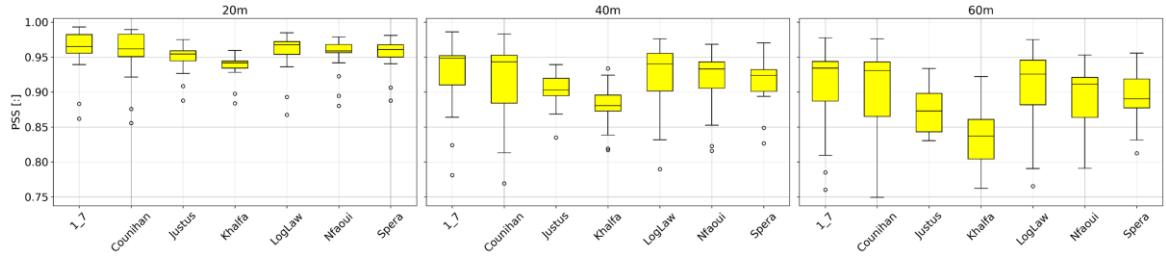

Figure 19: Boxplot of PSS comparison of scaling methods at multiple heights

III.2.2. Evaluation of the Simulated 10m scaled to different heights

The simulated 10 m wind speeds from ICON-LAM, ERA5 and ERA5_GWA are scaled to 20 m, 40 m, and 60 m using seven methods: 1_7_Law, Counihan_Law, Justus_Law,

Khalfa_Law, Nfaoui_Law and Spera_Law for ERA5_GWA, and ten methods: 1_7_Law, Counihan_Law, Justus_Law, Khalfa_Law, Nfaoui_Law, Spera_Law, Adv_Lin, Adv_Pl and Adv_Log for ICON-LAM and ERA5. Then Adv_Lin, Adv_Pl and Adv_Log are not used for ERA5_GWA. The influence of the datasets and the different height scaling methods on wind speed is highlighted by this analysis. For each metric, a box plot will display the results. The ICON-LAM dataset is represented by the red box, ERA5 by the blue box, and the green box represents the ERA5_GWA dataset. The results will focus on three datasets and three scaling methods, Adv_Lin, Adv_Pl, and Adv_Log, which were not discussed in the previous part.

The results of all methods are summarised in Table 15 (see the appendices)

III.2.2.1. MAE

In general, ERA5 demonstrates the highest levels of error with significant dispersion, while ICON-LAM and ERA5_GWA show the contrast, with ICON-LAM demonstrating a slight advantage over ERA5_GWA in terms of dispersion. The influence of the dataset is found to be more significant than that of the scaling methods. The findings demonstrate consistency in methods performance across the three scaling heights, except for Adv_Lin, Adv_Pl, and Adv_Log. The bias introduced by Adv_Lin, Adv_Pl, and Adv_Log decreases when we compare 10 m to 20 m scaling and 10 m to 40 m and increases when we consider a comparison of 10 m to 40 m scaling and 10 m to 60 m scaling. Adv_Lin introduced the highest bias of 3.57 m/s for the scaling from 10 m to 20 m, while Adv_Pl and Adv_Log exhibit a good performance compared to other methods. Figure 20 presents the MAE results with a box plot.

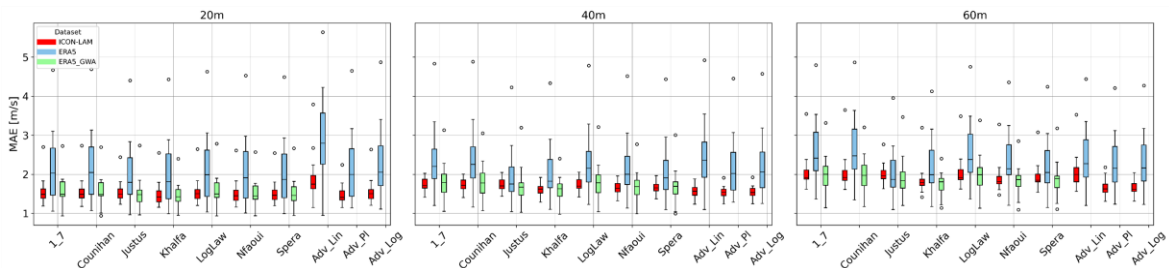

Figure 20: Boxplot of MAE for the datasets and the scaling methods comparison at multiple heights

III.2.2.2. ME

It is evident that ERA5 underestimates the scaled windspeed for all methods with high dispersion across different stations, while ICON-LAM and ERA5_GWA introduced a slight underestimation for all methods except the Justus_Law, which exhibits an overestimation. ERA5_GWA and ICON-LAM have similar performance across the same methods, with a small advantage for ICON-LAM. Figure 21 shows the ME results with a box plot. As for MAE, there is a consistency of method's performance across the three scaling heights, except for Adv_Lin, Adv_Pl, and Adv_Log, which depend on the specific scaling height. Within the methods, the Adv_Lin introduced the highest error with an underestimation of -2.2 m/s for ERA5 for a scaling from 10 m to 20 m. Adv_Pl and Adv_Log exhibit a good performance compared to other methods.

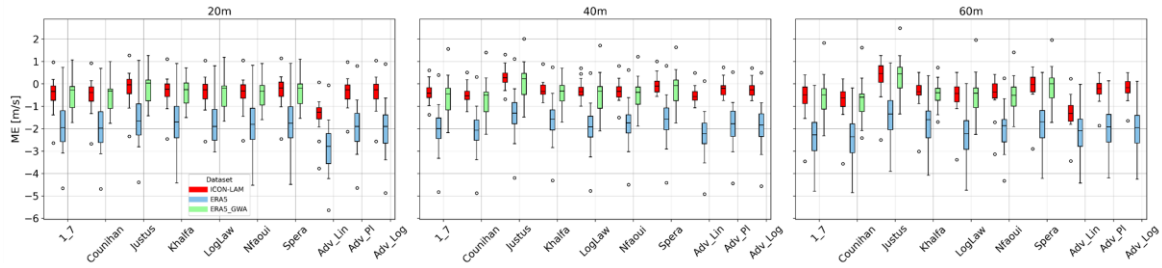

Figure 21: Boxplot of ME for the datasets and the scaling methods comparison at multiple heights

III.2.2.3. Pearson r

A Pearson correlation coefficient of similar value is recorded throughout the three datasets and across all methods.

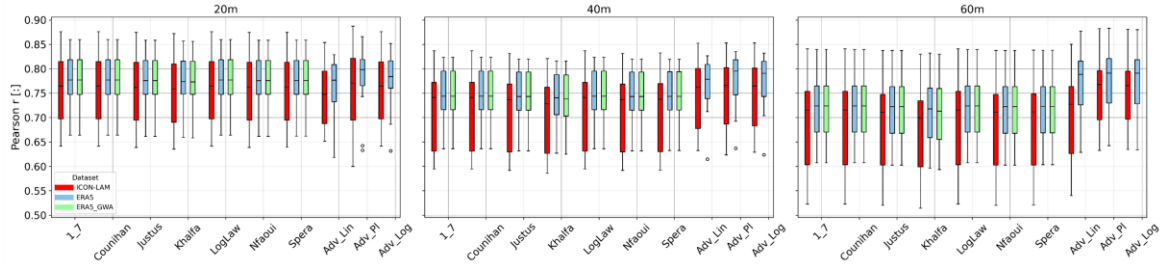

Figure 22: Boxplot of Pearson r for the datasets and the scaling methods comparison at multiple heights

The difference between dataset performance increase with the increases of the scaling height. Otherwise, the three datasets exhibited a substantial degree of dispersion. ERA5 and ERA5_GWA, which demonstrate a high correlation value, exhibit superior performance in comparison to ICON-LAM. The difference between methods within the same dataset is negligible. Figure 22 presents the Pearson correlation results for the dataset and scaling methods comparison.

For a scaling from 10 m to 20 m, the difference between dataset's performance is negligible. ICON-LAM show a correlation of around 0.81, while ERA5 and ERA5_GWA show a correlation of 0.82. For a scaling from 10 m to 40 m, ICON-LAM show a correlation between 0.76 and 0.80, while ERA5 and ERA5_GWA show a correlation between 0.79 and 0.82. Finally, for a scaling from 10 m to 60 m, ICON-LAM shows a correlation between 0.73 and 0.80, while ERA5 and ERA5_GWA show a correlation between 0.76 and 0.82

III.2.2.4. PSS

In general, ICON-LAM outperforms ERA5_GWA and ERA5 for each method, with a high PSS around 0.9 and the lowest dispersion. ERA5 shows the lowest performance for each method, with a high dispersion across different stations. There is also a consistency in method's performance across the three scaling heights. Adv_Pl and Adv_Log exhibit a good performance compared to other methods, while Adv_Lin recorded the lowest score of 0.7 for ERA5 for the scaling from 10 m to 20 m. Figure 23 presents the PSS results with a box plot.

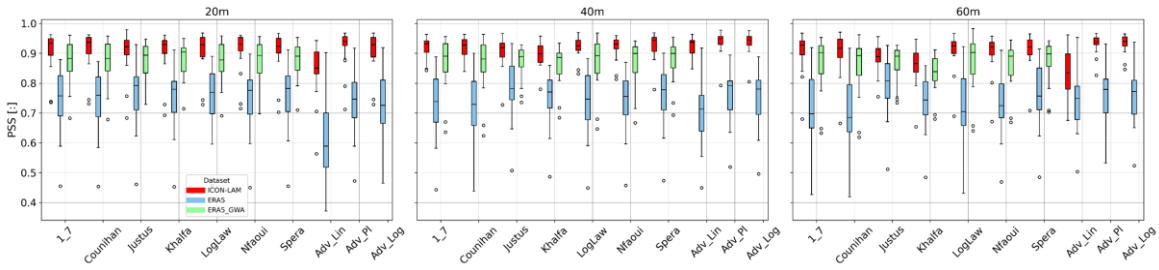

Figure 23: Boxplot of PSS for the datasets and the scaling methods comparison at multiple heights

III.2.3. Evaluation through a Taylor Diagram

A Taylor diagram is plotted for the three scaling heights 20 m, 40 m, and 60 m. Each of them combines both observed 10 m wind speeds scaled to different heights here, as obs_extra, and simulated 10 m wind speeds scaled to different heights. The ensuing plot serves as a crucial tool for the validation process, offering a comprehensive evaluation of the performance of all methods. 10 methods from ICON-LAM and ERA5, 7 methods from ERA5_GWA and Obs_extra are compared given a total of 34 methods. ICON-LAM methods are represented with red markers, ERA5 with blue markers, ERA5_GWA with green markers and Obs_extra with yellow markers. The name of the corresponding dataset is put at the end of the methods in the legend of every diagram to make a difference between methods from different datasets. The following Taylor diagrams are presented: the first, illustrated by Figure 24, is for the scaling from 10 m to 20 m, the second, by Figure 25, for the scaling from 10 m to 40 m, and the third, by Figure 26, for the scaling from 10 m to 60 m. A ranking table is provided, and it summarises the performance of each method from the three datasets at different scaling heights, from 10 m to 20 m by Table 11, from 10 m to 40 m by Table 12 and from 10 m to 60 m by Table 13.

In general, for every scaling height, methods from the 10 m observed wind speed scaled to different heights obtain the highest scores. This is because the impact of datasets is more significant than that of different methods, and the comparison is done against observed data. The lowest scores are obtained by the different methods from ERA5, due to a low standard deviation of ERA5's different methods, thereby confirming the high dispersion shown by the boxplots. ERA5_GWA and ICON-LAM demonstrate analogous performance, with ERA5_GWA exhibiting an advantage in scaling from 10 m to 20 m; however, this tendency undergoes a shift with increasing scaling height from 10 m to 40 m and from 10 m to 60 m. There are no trends in the performance of Adv_Lin, Adv_Pl, and Adv_Log regarding the scaling height, confirming the importance of the choice of the nearest height wind speed for those methods. However, Adv_Pl and Adv_Log exhibit a good performance compared to other methods, while Adv_Lin shows a contrast.

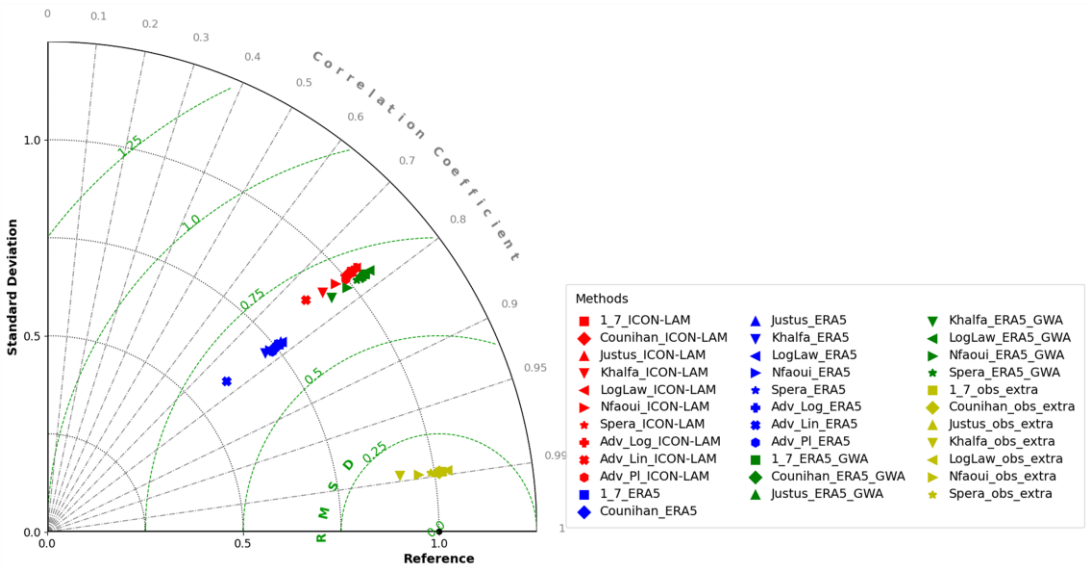

Figure 24: Taylor Diagram for 10m to 20m scaling

Table 11: Taylor Skill Score for 10m to 20m scaling

Scaling 10 m to 20 m

Methods	Scores	Methods	Scores
Justus_Law_obs_extra	0.994	Spera_ Law_ICON	0.879
Counihan_ Law_obs_extra	0.994	Adv_Log_ICON	0.879
Spera_ Law_obs_extra	0.994	LogLaw_ICON	0.879
1_7_ Law_obs_extra	0.994	Justus_ Law_ICON	0.879
LogLaw_obs_extra	0.993	Nfaoui_ Law_ICON	0.878
Nfaoui_ Law_obs_extra	0.992	Khalfa_ Law_ICON	0.873
Khalfa_ Law_obs_extra	0.985	Adv_Lin_ICON	0.860
Counihan_ Law_ERA5_GWA	0.887	LogLaw_ERA5	0.831
Spera_ Law_ERA5_GWA	0.887	Justus_ Law_ERA5	0.828
Nfaoui_ Law_ERA5_GWA	0.887	1_7_ Law_ERA5	0.825
1_7_ Law_ERA5_GWA	0.887	Counihan_ Law_ERA5	0.821
Justus_ Law_ERA5_GWA	0.887	Spera_ Law_ERA5	0.821
LogLaw_ERA5_GWA	0.886	Adv_Pl_ERA5	0.812
Khalfa_ Law_ERA5_GWA	0.883	Adv_Log_ERA5	0.809
Adv_Pl_ICON	0.882	Nfaoui_ Law_ERA5	0.807
Counihan_ Law_ICON	0.880	Khalfa_ Law_ERA5	0.797
1_7_ Law_ICON	0.879	Adv_Lin_ERA5	0.684

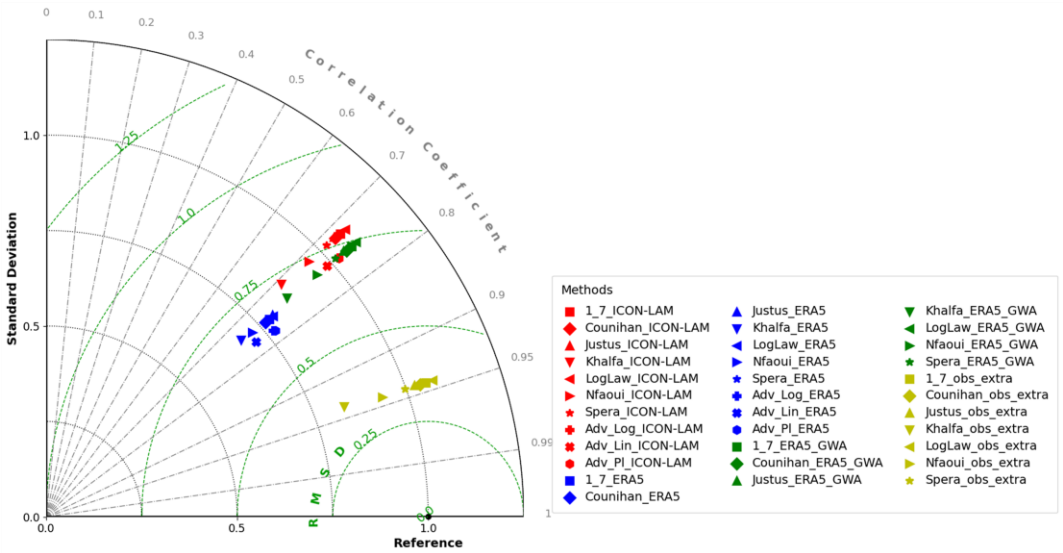

Figure 25: Taylor Diagram for 10m to 40m scaling

Table 12: Taylor Skill Score for 10m to 40m scaling

Scaling 10 m to 40 m

Methods	Scores	Methods	Scores
Spera_obs_extra	0.971	Counihan_ICON	0.858
Justus_obs_extra	0.970	Nfaoui_ICON	0.857
Counihan_obs_extra	0.970	Justus_ICON	0.856
1_7_obs_extra	0.969	1_7_ICON	0.856
LogLaw_obs_extra	0.967	LogLaw_ICON	0.854
Nfaoui_obs_extra	0.966	Khalfa_ERA5_GWA	0.847
Khalfa_obs_extra	0.936	Khalfa_ICON	0.837
Adv_Pl_ICON	0.874	Adv_Pl_ERA5	0.832
Adv_Log_ICON	0.874	LogLaw_ERA5	0.829
Adv_Lin_ICON	0.873	Justus_ERA5	0.828
Spera_ERA5_GWA	0.873	Adv_Log_ERA5	0.827
Counihan_ERA5_GWA	0.872	1_7_ERA5	0.822
Justus_ERA5_GWA	0.871	Counihan_ERA5	0.816
Nfaoui_ERA5_GWA	0.870	Spera_ERA5	0.815
1_7_ERA5_GWA	0.870	Adv_Lin_ERA5	0.792
LogLaw_ERA5_GWA	0.868	Nfaoui_ERA5	0.787
Spera_ICON	0.858	Khalfa_ERA5	0.759

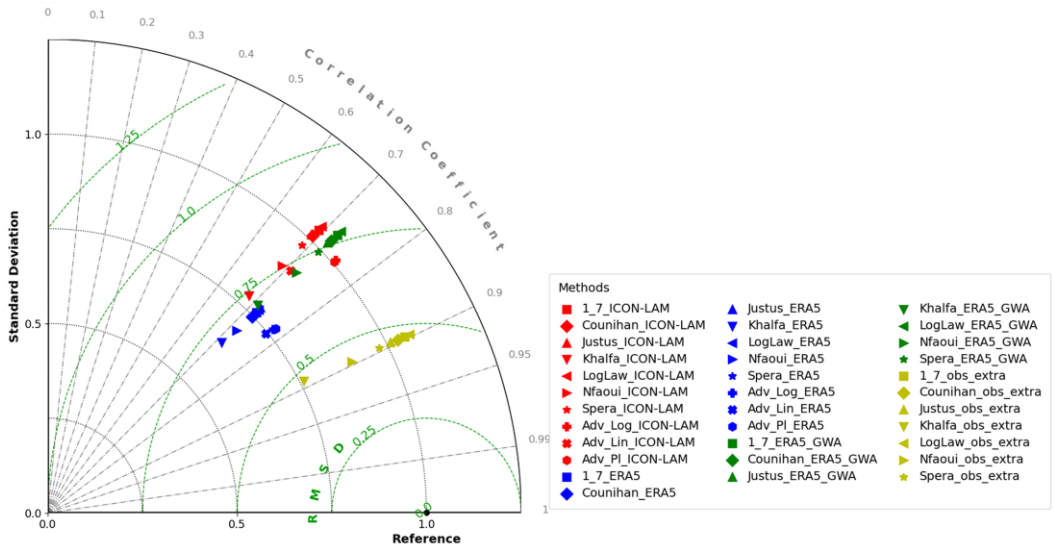

Figure 26: Taylor Diagram for 10m to 60m scaling

Table 13: Taylor Skill Score for 10m to 60m scaling

Scaling 10 m to 60 m

Methods	Scores	Methods	Scores
Justus_obs_extra	0.947	1_7_ICON	0.845
Counihan_obs_extra	0.947	LogLaw_ICON	0.844
Spera_obs_extra	0.947	Justus_ICON	0.844
1_7_obs_extra	0.946	Spera_ICON	0.844
LogLaw_obs_extra	0.944	Nfaoui_ICON	0.835
Nfaoui_obs_extra	0.937	Adv_Pl_ERA5	0.833
Khalfa_obs_extra	0.877	Adv_Log_ERA5	0.829
Adv_Pl_ICON	0.876	Adv_Lin_ERA5	0.814
Adv_Log_ICON	0.875	Justus_ERA5	0.809
Spera_ERA5_GWA	0.860	LogLaw_ERA5	0.806
Counihan_ERA5_GWA	0.860	Khalfa_ERA5_GWA	0.805
Justus_ERA5_GWA	0.859	1_7_ERA5	0.801
1_7_ERA5_GWA	0.858	Counihan_ERA5	0.791
LogLaw_ERA5_GWA	0.856	Spera_ERA5	0.791
Nfaoui_ERA5_GWA	0.852	Khalfa_ICON	0.791
Adv_Lin_ICON	0.846	Nfaoui_ERA5	0.753
Counihan_ICON	0.846	Khalfa_ERA5	0.709

III.3. Wind Power Simulation

The wind energy is estimated over the 3 years study time periods. As for the height scaling methods, the datasets and scaling method's impact on the wind power is investigated through two analyses. The first is the estimation of the wind energy density using the scaled wind speed from the observed 10m wind speed. The second is the use of the scaled wind speed from the 10m simulated wind speed to estimate the wind energy density. A cut-in and cut-out wind speed of respectively 2.0 m/s and 25.0 m/s is set on the observed wind speed, and a relative deviation boxplot helps for the analysis.

III.3.1. The impact of scaling methods wind speed on the power simulation

The direct impact of seven height scaling methods on wind power simulation is evaluated. A boxplot of the relative deviation of each methods, highlights in Figure 27, the systematic biases associated with the different scaling methods.

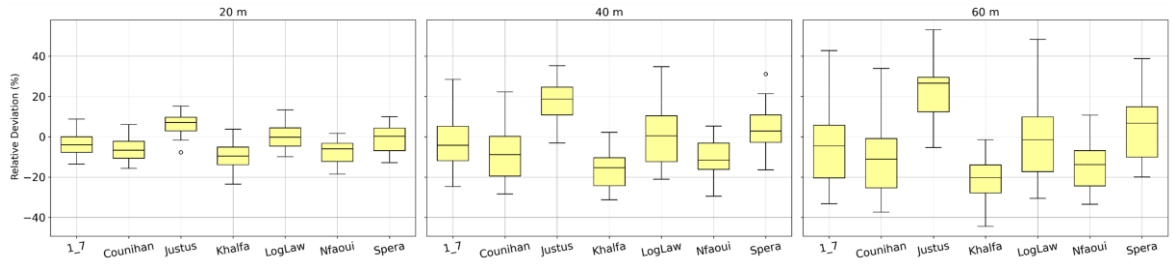

Figure 27: Boxplot of Energy Relative deviation for scaling methods wind energy estimation comparison at multiple height

In general, the increase in the scaling height led to an increase in the dispersion of wind energy estimation. While Justus_Law and Spera_Law overestimated the wind energy, Khalfa_Law and Nfaoui_Law exhibited an underestimation. In the case of 1_7_Law, Counihan_Law and LogLaw, a slight deviation was observed.

In the context of a scaling ranging from 10 m to 20 m, all the methods presented exhibited low dispersion. In contrast, Justus_Law, Spera_Law, and LogLaw exhibited an overestimation of energy, with errors of approximately 9.62%, 4.31% and 4.33%, respectively. Conversely, Counihan_Law, Khalfa_Law and Nfaoui_Law demonstrated an underestimation of energy, with errors of approximately 2.32%, 5.15% and 3.28%,

respectively. The 1_7_Law estimation demonstrated the most precise result, exhibiting a mere 0.03% energy discrepancy.

All methods exhibited an increase in dispersion when a scaling factor was applied, ranging from 10 m to 40 m. While Justus_Law, Spera_Law and LogLaw overestimated the energy, respectively, for approximately 24.58%, 10.79% and 10.37%, Khalfa_Law underestimated the energy for approximately 10.43%. The 1_7_Law and Counihan_Law exhibited a marginal overestimation of 5.21% and 0.11%, respectively. Nfaoui_Law exhibited a marginal underestimation of 3.22%.

It was evident that all methods presented a high degree of dispersion when a scaling factor ranging from 10 m to 60 m was employed. While Justus_Law, Spera_Law and LogLaw respectively exhibited an overestimation of 29.53%, 14.87% and 9.85%, Khalfa_Law and Nfaoui_Law underestimated the wind energy estimation by 14% and 6.96%, respectively. Finally, the 1_7_Law exhibited a marginal overestimation of 5.69% and the Counihan_Law demonstrated a slight underestimation of around 0.88%.

III.3.2. The impact of datasets and scaling methods wind speed on the power simulation

The impact of both datasets and scaling methods on wind power simulation is evaluated. A boxplot of the relative deviation of each methods, highlights in Figure 28 the systematic biases associated with the different datasets and scaling methods. The ICON-LAM dataset is represented with red box, ERA5 with blue box and ERA5_GWA with green box.

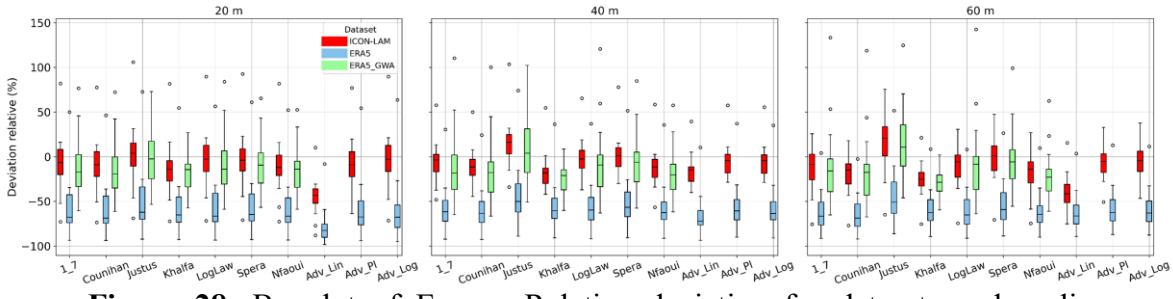

Figure 28: Boxplot of Energy Relative deviation for datasets and scaling methods wind energy estimation comparison at multiple height

In general, ERA5 underestimates wind energy, with a high degree of dispersion being observed across different weather mast stations. ICON-LAM and ERA5_GWA have been shown to have similar estimation properties, with ICON-LAM demonstrating an advantage in terms of low dispersion when compared to ERA5_GWA. The impact of the dataset is found to be of greater significance than that of the scaling methods. Analogous trends were observed at the various scaling heights. The following essay will provide a comprehensive overview of the relevant literature on the subject.

The ERA5 model demonstrates an underestimation of wind energy estimation ranging from 33.83% for Justus_Law to 75% for Adv_Lin, when scaling is conducted from 10 m to 20 m. The Adv_Pl and the Adv_Log exhibited an underestimation of 49.34% and 54.06%, respectively. With ICON-LAM, Justus_Law exhibited an overestimation of wind energy by approximately 15.42%, while Adv_Lin underestimated the wind energy by 36%. The Adv_Pl and the Adv_Log respectively presented an overestimation of 5.60% and 12.57%, respectively. With ERA5_GWA, Justus_Law exhibited an overestimation of wind energy by approximately 17.48%, while Khalfa_Law demonstrated an underestimation of wind energy by around 8.16%.

For a scaling for 10 m to 40 m, ERA5 show an underestimation of wind energy estimation between 30.17% for Justus_Law and 60.33% for Adv_Lin. Adv_Pl and Adv_Log presented respectively an underestimation of 48.01% and 50.30%. With ICON-LAM, Justus_Law overestimated the wind energy for about 24.81% while Adv_Lin underestimated the wind energy for about 11.27%. Adv_Pl and Adv_Log presented respectively an overestimation of 2.74% and 2.07%. With ERA5_GWA, Justus_Law overestimated the wind energy for about 31.16% while Khalfa_Law underestimated the wind energy for about 14.57%.

For a scale ranging from 10 m to 60 m, the ERA5 model demonstrates an underestimation of wind energy estimation, with a range of 28.16% to 54.15% for Justus_Law and Adv_Lin, respectively. The results of the Adv_Pl and Adv_Log models indicated an underestimation of 48.03% and 49.60%, respectively. It is evident that ICON-LAM led to an overestimation of wind energy by approximately 33.56% by Justus_Law, while Adv_Lin resulted in an underestimation of wind energy by around 30.93%. It was demonstrated that both Adv_Pl and Adv_Log exhibited an overestimation of 3.25% and 6.18%, respectively. Utilising ERA5_GWA, Justus_Law exhibited an overestimation of wind energy by approximately 35.68%, while Khalfa_Law demonstrated an underestimation of wind energy by around

20.50%.

Conclusion

In this chapter, all result from every evaluation were presented. The accuracy of datasets and height scaling methods was evaluated throughout three evaluations. First the simulated 10 m wind speed from three dataset were compared against the observation. After the accuracy of dataset and scaling method were evaluated in multiple height wind speed estimation. Finally, the impact on wind power production were evaluated. The upcoming part of this study is the conclusion and futures perspectives.

CONCLUSION AND PERSPECTIVES

CONCLUSION AND PERSPECTIVES

This study investigates the impact of wind data variant on the wind power simulation by first evaluating the accuracy of atmospheric numerical datasets ICON-LAM, ERA5 and ERA5_GWA to simulate 10m wind speed over 204 meteorological stations from TAHMO, SASSCAL_WN and NCEI_ISD across the Southern Africa, second evaluating the accuracy of both dataset and 10 height scaling methods to estimate multiple heights 20 m, 40 m and 60 m wind speed over 18 weather mast stations from WASA across South Africa, and finally to evaluate the impact of both datasets and scaling methods on wind energy estimation over 18 weather mast stations from WASA across South Africa.

The datasets accuracy comparison on 10 m wind speed was done using 4 metrics MAE, ME, Pearson r and PSS and the results show that ERA5_GWA introduced the lowest bias, with the lowest overestimation and the highest frequency distribution overlapping area of the 10m wind speed while ICON-LAM introduced the opposites. However, the three datasets have similar correlation of 10m wind speed simulation with a slight advantage of ICON-LAM on ERA5 and ERA5_GWA which have the same correlation. Therefore, ERA5_GWA well simulated the 10 m wind speed across the Southern Africa compared to ERA5 and ICON-LAM. Else, the statistical downscaling with the GWA, on ERA5, to produce ERA5_GWA, introduced a bias correction and improved the simulation accuracy shown by ERA5_GWA. The performance of ICON-LAM is comparable to others study Chen et al., 2024a.

The datasets and height scaling accuracy comparison on multi height wind speed was done through two analyses using 4 metrics and a Talyor Diagram. In the first analysis, the observed 10 m wind speed is scaled to 20 m, 40 m and 60 m using seven 07 height scaling methods 1_7_Law, LogLaw, Counihan_Law, Justus_Law, Khalfa_Law, Nfaoui_Law and Spera_Law, and those scaled wind speeds are compared against the observed wind speed at 20 m, 40 m, and 60 m. This allows to evaluate the accuracy of the scaling method only and the results show that, for all methods the errors introduced, and the dispersion increase with the scaling height. At 20 m, the bias difference between methods and dispersion are small then difficult to distinguished, but at 60 m, these bias differences are more visible, and the dispersion are high. While all methods tend to underestimate the wind speed, Justus_Law, and Spera_Law trend to overestimate the wind speed. 1_7_Law and Counihan_Law show a satisfactory performance on wind speed estimation. In the second

analysis, the simulated 10 m wind speed is scaled to 20 m, 40 m and 60 m using ten 10 height scaling methods 1_7_Law, LogLaw, Counihan_Law, Justus_Law, Khalfa_Law, Nfaoui_Law, Spera_Law, Adv_Lin, Adv_Pl and Adv_Log except for ERA5_GWA which use the seven 07 previous height scaling methods. Those scaled wind speeds are compared against the observed wind speed at 20 m, 40 m, and 60 m. This allows to evaluate the accuracy of both datasets and the scaling methods, and the results show that, the impact of datasets prior that of scaling methods, with ERA5 models which clearly underestimated the wind speed. ICON-LAM and ERA5_GWA have similar performance with a slight advantages of ICON-LAM. A same trend was observed for all methods and datasets during the three-scaling range, except Adv_Lin, Adv_Pl, and Adv_Log. The performance of those three methods show that the choice of nearest reference heights impacts the accuracy of the estimation. The results obtained are comparable with others study Chen et al. 2024b.

The impact of datasets and height scaling methods on the wind power simulation was also that through two analyses. The First, show the direct impact of height scaling methods on wind power simulation, where the observed 10 m wind speed, scaled to 20 m, 40 m and 60 m using the seven 07 previous height scaling methods, are used for the wind energy estimation over the 3 years. The result followed the same trend as that of the wind speed estimation. 1_7_Law and Counihan_Law have a satisfactory performance with a marginal overestimation of 5.69% and a slight underestimation of 0.88%, respectively. The last analysis shows the impact of both dataset and scaling methods on wind power simulation. Similar, the accuracy of the estimation followed the same trend as that of the wind speed estimation. ERA5 critically underestimated the wind energy for Adv_Lin, of up to 54.15% in the context of a scaling from 10 m to 60 m and of up to 75% in the context of a scaling from 10 m to 20 m. Advanced Law highly depend on the choice of nearest reference heights. Else, the results of ICON-LAM for Adv_Lin -36% compared to Adv_Pl +5.60% and Adv_Log +12.57% in the context of a scaling from 10 m to 20 m shows Adv_Lin did not well estimate the wind speed and the wind energy as it do not take into account, the atmosphere stability and surface roughness impacts.

All in all, this study reveals the performance of different wind speed height scaling methods to scale wind speed from 10 m to multiple heights and how this would impact on the subsequent wind power calculation. Similar results are found using different wind speed scaling methods, while the choice of the numerical atmospheric data set seems more to be

the decisive factor on the accuracy of wind speed and wind power calculation.

One of the constraints is the limited study area of the wind power simulation. Only the 18 weather mast stations available data were used. More weather mast stations imply more locations, more wind turbine locations or in general more potential wind farm locations which could have been investigated for a better validation of the results. Another constraint of this study is the limited time span which is only 3 years from 2017 to 2019. A large time span could allow the coverage of more climate events which will influence the outputs of this study as the wind speed will be impacted. Finally, this study did not include any real wind turbines. The wind power simulation comparison of this study did not use any available real wind turbine power generation data for a comparison against dataset and methods simulation data. This could enhance the study results as real wind turbine involved a parameter such as the turbine efficiency and the capacity factors, which affect a lot the wind power and are critical parameters for policy makers.

Therefore, the future perspective of this current study is it expansion to a global scale. The datasets and methods accuracy could be investigated over an entire continent such as Africa, during a study period of 10 years and more. This will help to highlight the interannual variability, the climate impact as well as regional impact on wind power simulation. Else, the study could include the use of weather mast stations, which measurement height are close to modern wind turbines hub height i.e., 100 m, which will put the study close to real-life situations and increase the accuracy of the results.

BIBLIOGRAPHY

Abbas, Q., Khan, A. R., Bashir, A., Alemzero, D. A., Sun, H., Iram, R., & Iqbal, N. 2020. Scaling up renewable energy in Africa: measuring wind energy through econometric approach. *Environmental Science and Pollution Research*, *27*29, 36282–36294. https://doi.org/10.1007/S11356-020-09596-1/TABLES/4

Agbetuyi, A. F., Odigwe, I. A., Awelewa, A., & Awosope, C. 2013. Wind power potential and integration in Africa. *International Journal of Development and Sustainability*, *2*1, 232–239. https://www.isdsnet.com/ijds-v2n1-16.pdf

Aminzadeh, A., Dimitrova, M., Meiabadi, M. S., Sattarpanah Karganroudi, S., Taheri, H., Ibrahim, H., & Wen, Y. 2023. Non-Contact Inspection Methods for Wind Turbine Blade Maintenance: Techno–Economic Review of Techniques for Integration with Industry 4.0. *Journal of Nondestructive Evaluation*, *42*2. https://doi.org/10.1007/S10921-023-00967-5

Ashkenazy, Y., & Yizhaq, H. 2023. The diurnal cycle and temporal trends of surface winds. *Earth and Planetary Science Letters*, *601*, 117907. https://doi.org/10.1016/J.EPSL.2022.117907

Badger, J., & Jørgensen, H. E. 2011. A high resolution global wind atlas - improving estimation of world wind resources. *Energy Systems and Technologies for the Coming Century*, 215–225. https://orbit.dtu.dk/en/publications/a-high-resolution-global-wind-atlas-improving-estimation-of-world

Bagavathsingh, A., Srinivas, C. V., Maran Sardar, P., Baskaran, R., & Venkatraman, B. 2016. No Title. *International Journal of Geology, Agriculture and Environmental Sciences*, *4*3.

Barthelmie, R. J., Wang, H., Doubrawa, P., & Pryor, S. C. 2016. *Best Practice for Measuring Wind Speeds and Turbulence Offshore through In-situ and Remote Sensing Technologies*.

Bollmeyer, C., Keller, J. D., Ohlwein, C., Wahl, S., Crewell, S., Friederichs, P., Hense, A., Keune, J., Kneifel, S., Pscheidt, I., Redl, S., & Steinke, S. 2015. Towards a high-resolution regional reanalysis for the European CORDEX domain. *Quarterly Journal of the Royal Meteorological Society*, *141*686, 1–15. https://doi.org/10.1002/QJ.2486

Brönnimann, S., Allan, R., Atkinson, C., Buizza, R., Bulygina, O., Dahlgren, P., Dee, D., Dunn, R., Gomes, P., John, V. O., Jourdain, S., Haimberger, L., Hersbsbach, H.,

Kennedy, J., Poli, P., Pulliainen, J., Rayner, N., Saunders, R., Schulz, J., … Wilkinson, C. 2018. Observations for Reanalyses. *Bulletin of the American Meteorological Society*, *999*, 1851–1866. https://doi.org/10.1175/BAMS-D-17-0229.1

Bulut, A., & Bingöl, O. 2024. Weibull parameter estimation methods on wind energy applications - a review of recent developments. *Theoretical and Applied Climatology 2024 155:10*, *155*10, 9157–9184. https://doi.org/10.1007/S00704-024-05184-2

Burton, T., Jenkins, N., Sharpe, D., & Bossanyi, E. 2011. *Wind Energy: Handbook* 2nd ed.. John Wiley & Sons, Ltd.

Carta, J. A., Ramírez, P., & Velázquez, S. 2009. A review of wind speed probability distributions used in wind energy analysis: Case studies in the Canary Islands. *Renewable and Sustainable Energy Reviews*, *135*, 933–955. https://doi.org/10.1016/J.RSER.2008.05.005

Cerralbo, P., Grifoll, M., Moré, J., Bravo, M., Sairouní Afif, A., & Espino, M. 2015. Wind variability in a coastal area Alfacs Bay, Ebro River delta. *Advances in Science and Research*, *12*1, 11–21. https://doi.org/10.5194/ASR-12-11-2015

Charabi, Y., Al-Yahyai, S., & Gastli, A. 2011. Evaluation of NWP performance for wind energy resource assessment in Oman. *Renewable and Sustainable Energy Reviews*, *15*3, 1545–1555. https://doi.org/10.1016/j.rser.2010.11.055

Chen, S., Goergen, K., Hendricks Franssen, H. J., Winkler, C., Poll, S., Houssoukri Zounogo Wahabou, Y., Linssen, J., Vereecken, H., Stolten, D., & Heinrichs, H. 2024. Higher Onshore Wind Energy Potentials Revealed by Kilometer-Scale Atmospheric Modeling. *Geophysical Research Letters*, *51*19, e2024GL110122. https://doi.org/10.1029/2024GL110122;WGROUP:STRING:PUBLICATION

Chen, S., Poll, S., Hendricks Franssen, H. J., Heinrichs, H., Vereecken, H., & Goergen, K. 2024. Convection-Permitting ICON-LAM Simulations for Renewable Energy Potential Estimates Over Southern Africa. *Journal of Geophysical Research: Atmospheres*, *129*6, 1–29. https://doi.org/10.1029/2023JD039569

Chirachawala, C., Shrestha, S., Babel, M. S., Virdis, S. G. P., & Wichakul, S. 2020. Evaluation of global land use/land cover products for hydrologic simulation in the Upper Yom River Basin, Thailand. *Science of The Total Environment*, *708*, 135148. https://doi.org/10.1016/J.SCITOTENV.2019.135148

Coppola, E., Giorgi, F., Giuliani, G., Pichelli, E., Ciarlo`, J. M., Raffaele, F., Nogherotto,

R., Reboita, M. S., Lu, C., Zazulie, N., Vargas-Heinz, L., Cardoso, A. A., & Leeuw, J. de. 2024. The Fifth Generation Regional Climate Modeling System, RegCM5: the first CP European wide simulation and validation over the CORDEX-CORE domains. *ESS Open Archive Eprints*, *899*, 170542078–180092084. https://doi.org/10.22541/ESSOAR.170542078.80092084/V1

Counihan, J. 1975. Adiabatic atmospheric boundary layers: a review and analysis of data collected from the period 1880–1972. *Atmospheric Environment*, *9*, 871–905.

Crippa, P., Alifa, M., Bolster, D., Genton, M. G., & Castruccio, S. 2021. A temporal model for vertical extrapolation of wind speed and wind energy assessment. *Applied Energy*, *301*, 117378. https://doi.org/10.1016/J.APENERGY.2021.117378

Dahham, A. W., Kasenov, A. Z., Aljibory, M. W., Hilal, M. M., Abishev, K. K., Kereyovna, M. Z., Sembayev, N. S., Dahham, H. W., Bykov, P. O., & Alirakhimovich, A. A. 2023. Design parameters and mechanical efficiency of jet wind turbine under high wind speed conditions. *Open Engineering*, *13*1. https://doi.org/10.1515/ENG-2022-0450/ASSET/GRAPHIC/J_ENG-2022-0450_FIG_008.JPG

Davis, N. N., Badger, J., Hahmann, A. N., Hansen, B. O., Mortensen, N. G., Kelly, M., Larsén, X. G., Olsen, B. T., Floors, R., Lizcano, G., Casso, P., Lacave, O., Bosch, A., Bauwens, I., Knight, O. J., Potter van Loon, A., Fox, R., Parvanyan, T., Krohn Hansen, S. B., … Drummond, R. 2023. The Global Wind Atlas: A High-Resolution Dataset of Climatologies and Associated Web-Based Application. *Bulletin of the American Meteorological Society*, *104*8, E1507–E1525. https://doi.org/10.1175/BAMS-D-21-0075.1

Devis, A., Van Lipzig, N. P. M., & Demuzere, M. 2018. Should future wind speed changes be taken into account in wind farm development? *Environmental Research Letters*, *13*6, 064012. https://doi.org/10.1088/1748-9326/AABFF7

dos Santos Silva, F. D., da Costa, C. P. W., dos Santos Franco, V., Gomes, H. B., da Silva, M. C. L., dos Santos Vanderlei, M. H. G., Costa, R. L., da Rocha Júnior, R. L., Cabral Júnior, J. B., dos Reis, J. S., Cavalcante, R. B. L., Tedeschi, R. G., de Jesus da Costa Barreto, N., Nogueira Neto, A. V., dos Santos Jesus, E., & da Silva Ferreira, D. B. 2023. Intercomparison of Different Sources of Precipitation Data in the Brazilian Legal Amazon. *Climate*, *11*12, 241. https://doi.org/10.3390/CLI11120241/S1

Duranay, Z. B., Güldemir, H., & Coşkun, B. 2024. The Role of Wind Turbine Siting in

Achieving Sustainable Energy Goals. *Processes*, *12*12, 2900. https://doi.org/10.3390/PR12122900

Elkodama, A., Ismaiel, A., Abdellatif, A., Shaaban, S., Yoshida, S., & Rushdi, M. A. 2023. Control Methods for Horizontal Axis Wind Turbines HAWT: State-of-the-Art Review. *Energies*, *16*17, 6394. https://doi.org/10.3390/EN16176394

Elsner, P. 2019. Continental-scale assessment of the African offshore wind energy potential: Spatial analysis of an under-appreciated renewable energy resource. *Renewable and Sustainable Energy Reviews*, *104*, 394–407. https://doi.org/10.1016/J.RSER.2019.01.034

Emeis, S. 2018. *Wind Energy Meteorology Atmospheric Physics for Wind Power Generation* 2nd ed.. Springer Nature. https://doi.org/https://doi.org/10.1007/978-3-319-72859-9

Emeis, S., & Turk, M. 2007. Comparison of Logarithmic Wind Profiles and Power Law Wind Profiles and their Applicability for Offshore Wind Profiles. *Wind Energy*, 61–64. https://doi.org/10.1007/978-3-540-33866-6_11

Energy Institute. 2025. *Share of direct primary energy consumption by source, World, 2024*. Statistical Review of World Energy. https://ourworldindata.org/grapher/share-of-primary-energy-consumption-by-source?tab=discrete-bar&time=2024

Farrugia, R. N. 2003. The wind shear exponent in a Mediterranean island climate. *Renewable Energy*, *28*4, 647–653. https://doi.org/10.1016/S0960-14810200066-6

Fleming, P. D., & Probert, S. D. 1984. The evolution of wind-turbines: An historical review. *Applied Energy*, *18*3, 163–177. https://doi.org/10.1016/0306-26198490007-2

Foli, B. A. K., Appeaning Addo, K., Ansong, J. K., & Wiafe, G. 2022. Evaluation of ECMWF and NCEP Reanalysis Wind Fields for Long-Term Historical Analysis and Ocean Wave Modelling in West Africa. *Remote Sensing in Earth Systems Sciences*, *5*1–2, 26–45. https://doi.org/10.1007/S41976-021-00052-3/TABLES/5

Frank, C. W., Pospichal, B., Wahl, S., Keller, J. D., Hense, A., & Crewell, S. 2020. The added value of high resolution regional reanalyses for wind power applications. *Renewable Energy*, *148*, 1094–1109. https://doi.org/10.1016/J.RENENE.2019.09.138

Gbode, I. E., Babalola, T. E., Diro, G. T., & Intsiful, J. D. 2023. Assessment of ERA5 and ERA-Interim in Reproducing Mean and Extreme Climates over West Africa. *Advances in Atmospheric Sciences*, *40*4, 570–586. https://doi.org/10.1007/S00376-

022-2161-8

Gelaro, R., McCarty, W., Suárez, M. J., Todling, R., Molod, A., Takacs, L., Randles, C. A., Darmenov, A., Bosilovich, M. G., Reichle, R., Wargan, K., Coy, L., Cullather, R., Draper, C., Akella, S., Buchard, V., Conaty, A., da Silva, A. M., Gu, W., … Zhao, B. 2017. The Modern-Era Retrospective Analysis for Research and Applications, Version 2 MERRA-2. *Journal of Climate*, *30*14, 5419–5454. https://doi.org/10.1175/JCLI-D-16-0758.1

Gerland, P., Hertog, S., Wheldon, M., Kantorova, V., Gu, D., Gonnella, G., Williams, I., Zeifman, L., Bay, G., Castanheira, H., Kamiya, Y., Bassarsky, L., Gaigbe-Togbe, V., & Spoorenberg, T. 2022. *World Population Prospects 2022: Summary of results*. United Nations. https://www.researchgate.net/publication/361944109_World_Population_Prospects_2022_Summary_of_results

Ghoneam, S. M., Hamada, A. A., & Sherif, T. S. 2024. Fatigue-Life Estimation of Vertical-Axis Wind Turbine Composite Blades Using Modal Analysis. *Journal of Energy Resources Technology*, *146*3. https://doi.org/10.1115/1.4064178/1171662

Gipe, P. 1991. Wind energy comes of age California and Denmark. *Energy Policy*, *19*8, 756–767. https://doi.org/10.1016/0301-42159190045-P

Global Wind Atlas-Methodology. 2023. https://globalwindatlas.info/en/about/method

González-Aparicio, I., Monforti, F., Volker, P., Zucker, A., Careri, F., Huld, T., & Badger, J. 2017. Simulating European wind power generation applying statistical downscaling to reanalysis data. *Applied Energy*, *199*, 155–168. https://doi.org/10.1016/J.APENERGY.2017.04.066

Gorla, R., Pallikonda, M. K., & Walunj, G. 2020. Use of Rayleigh Distribution Method for Assessment of Wind Energy Output in Cleveland–Ohio. *Renewable Energy Research and Applications*, *1*1, 11–18. https://doi.org/10.22044/RERA.2019.1601

Gruber, K., Regner, P., Wehrle, S., Zeyringer, M., & Schmidt, J. 2021. Towards global validation of wind power simulations: A multi-country assessment of wind power simulation from MERRA-2 and ERA-5 reanalyses bias-corrected with the global wind atlas. *Energy*, *238*. https://doi.org/10.1016/J.ENERGY.2021.121520

Gualtieri, G., & Secci, S. 2011. Comparing methods to calculate atmospheric stability-dependent wind speed profiles: A case study on coastal location. *Renewable Energy*,

*36*8, 2189–2204. https://doi.org/10.1016/J.RENENE.2011.01.023

Gumuła, S., Piaskowska-Silarska, M., Pytel, K., Noga, H., & Kulinowski, W. 2017. Evaluation of the impact of adjusting the angle of the axis of a wind turbine rotor relative to the flow of air stream on operating parameters of a wind turbine model. *E3S Web of Conferences*, *14*, 01016. https://doi.org/10.1051/E3SCONF/20171401016

Haidi, T., & Cheddadi, B. 2022. Wind energy integration in Africa: development, impacts and barriers. *International Journal of Electrical and Computer Engineering*, *12*5, 4614–4622. https://doi.org/10.11591/ijece.v12i5.pp4614-4622

Hartmann, H. 2025a. Comparison of Precipitation Rates from Global Datasets for the Five-Year Period from 2019 to 2023. *Hydrology 2025, Vol. 12, Page 4*, *12*1, 4. https://doi.org/10.3390/HYDROLOGY12010004

Hartmann, H. 2025b. Comparison of Precipitation Rates from Global Datasets for the Five-Year Period from 2019 to 2023. *Hydrology 2025, Vol. 12, Page 4*, *12*1, 4. https://doi.org/10.3390/HYDROLOGY12010004

Haupt, S. E., & Mahoney, W. P. 2015. Taming wind power with better forecasts. *IEEE Spectrum*, *52*11, 47–53. https://doi.org/10.1109/MSPEC.2015.7335902

Hersbach, H., Bell, B., Berrisford, P., Hirahara, S., Horányi, A., Muñoz-Sabater, J., Nicolas, J., Peubey, C., Radu, R., Schepers, D., Simmons, A., Soci, C., Abdalla, S., Abellan, X., Balsamo, G., Bechtold, P., Biavati, G., Bidlot, J., Bonavita, M., … Thépaut, J. 2020. The ERA5 global reanalysis. *Quarterly Journal of the Royal Meteorological Society*, *146*730, 1999–2049. https://doi.org/10.1002/QJ.3803’

Holechek, J. L., Geli, H. M. E., Sawalhah, M. N., & Valdez, R. 2022. A Global Assessment: Can Renewable Energy Replace Fossil Fuels by 2050? *Sustainability Switzerland*, *14*8, 1–22. https://doi.org/10.3390/su14084792

Hu, W., Letson, F., Barthelmie, R. J., & Pryor, S. C. 2018. Wind Gust Characterization at Wind Turbine Relevant Heights in Moderately Complex Terrain. *Journal of Applied Meteorology and Climatology*, *57*7, 1459–1476. https://doi.org/10.1175/JAMC-D-18-0040.1

IEA. 2025a. *Global Energy Review 2025*. https://www.iea.org/reports/global-energy-review-2025#overview

IEA. 2025b. *World Energy Investment 2025-Africa*. https://www.iea.org/reports/world-energy-investment-2025

IRENA. 2025. *Renewable capacity statistics 2025*. International Renewable Energy Agency. https://www.irena.org/-/media/Files/IRENA/Agency/Publication/2025/Mar/IRENA_DAT_RE_Capacity_Statistics_2025.pdf

Iriza-Burcă, A., Dumitrache, R. C., Maco, B. A., Huştiu, M., Fundel, F., Rieger, D., Potthast, R., Iriza-Burcă, A., Dumitrache, R. C., Maco, B. A., Huştiu, M., Fundel, F., Rieger, D., & Potthast, R. 2024. Comparison of COSMO and ICON-LAM high-resolution numerical forecast for Romanian territory: Case studies and evaluation. *Atmósfera*, *38*, 421–451. https://doi.org/10.20937/ATM.53305

Jourdier, B., Diaz, C., & Dubus, L. 2023. Evaluation of CERRA for wind energy applications. *EMS Annual Meeting 2023*, *EMS2023-31*. https://doi.org/doi.org/10.5194/ems2023-311, 2023. 1

Jung, C., & Schindler, D. 2021. The role of the power law exponent in wind energy assessment: A global analysis. *International Journal of Energy Research*, *45*6, 8484–8496. https://doi.org/10.1002/ER.6382

Justus, C. G., & Mikhail, A. 1976. Height variation of wind speed and wind distributions statistics. *Geophysical Research Letters*, *3*5, 261–264. https://doi.org/10.1029/GL003I005P00261;PAGE:STRING:ARTICLE/CHAPTER

Kaldellis, J. K., & Zafirakis, D. 2011. The wind energy revolution: A short review of a long history. *Renewable Energy*, *36*7, 1887–1901. https://doi.org/10.1016/J.RENENE.2011.01.002

Kara, T., & Sahin, A. D. 2023. Implications of Climate Change on Wind Energy Potential. *Sustainability*, *15*20, 14822. https://doi.org/10.3390/SU152014822

Kassa, B. Y., Baheta, A. T., & Beyene, A. 2024. Current Trends and Innovations in Enhancing the Aerodynamic Performance of Small-Scale, Horizontal Axis Wind Turbines: A Review. *ASME Open Journal of Engineering*, *3*, 18. https://doi.org/10.1115/1.4064141

Kent, C. W., Lee, K., Ward, H. C., Hong, J. W., Hong, J., Gatey, D., & Grimmond, S. 2017. Aerodynamic roughness variation with vegetation: analysis in a suburban neighbourhood and a city park. *Urban Ecosystems 2017 21:2*, *212*, 227–243. https://doi.org/10.1007/S11252-017-0710-1

Khalfa, D., Benretem, A., Herous, L., & Meghlaoui, I. 2014. Evaluation of the adequacy of

the wind speed extrapolation laws for two different roughness meteorological sites. *American Journal of Applied Sciences*, *11*4, 570–583. https://doi.org/10.3844/ajassp.2014.570.583

Klaas-Witt, T., & Emeis, S. 2022. The five main influencing factors for lidar errors in complex terrain. *Wind Energy Science*, *7*1, 413–431. https://doi.org/10.5194/WES-7-413-2022,

Kobayashi, S., Ota, Y., Harada, Y., Ebita, A., Moriya, M., Onoda, H., Onogi, K., Kamahori, H., Kobayashi, C., Endo, H., Miyaoka, K., & Kiyotoshi, T. 2015. The JRA-55 reanalysis: General specifications and basic characteristics. *Journal of the Meteorological Society of Japan*, *93*1, 5–48. https://doi.org/10.2151/jmsj.2015-001

Koch, W., & Feser, F. 2006. Relationship between SAR-Derived Wind Vectors and Wind at 10-m Height Represented by a Mesoscale Model. *Monthly Weather Review*, *134*5, 1505–1517. https://doi.org/10.1175/MWR3134.1

Lee, J. T., Kim, H. G., Kang, Y. H., & Kim, J. Y. 2019. Determining the Optimized Hub Height of Wind Turbine Using the Wind Resource Map of South Korea. *Energies 2019, Vol. 12, Page 2949*, *12*15, 2949. https://doi.org/10.3390/EN12152949

Liu, Y., Warner, T., Liu, Y., Vincent, C., Wu, W., Mahoney, B., Swerdlin, S., Parks, K., & Boehnert, J. 2011. Simultaneous nested modeling from the synoptic scale to the LES scale for wind energy applications. *Journal of Wind Engineering and Industrial Aerodynamics*, *99*4, 308–319. https://doi.org/10.1016/J.JWEIA.2011.01.013

Løvøy Alvestad, B. P., Fevang-Gunn, L., Panjwani, B., & Bracchi, T. K. 2024. Effect of Atmospheric Stability on Meandering and Wake Characteristics in Wind Turbine Fluid Dynamics. *Applied Sciences 2024, Vol. 14, Page 8025*, *14*17, 8025. https://doi.org/10.3390/APP14178025

Mahoney, W. P., Parks, K., Wiener, G., Liu, Y., Myers, W. L., Sun, J., Delle Monache, L., Hopson, T., Johnson, D., & Haupt, S. E. 2012. A wind power forecasting system to optimize grid integration. *IEEE Transactions on Sustainable Energy*, *3*4, 670–682. https://doi.org/10.1109/TSTE.2012.2201758

Manco, I., De Lucia, C., Repola, F., Fedele, G., & Mercogliano, P. 2023. A Comparative Performance Study of WRF, COSMO and ICON Atmospheric Models for the Italian Peninsula at Very High Resolution. *Tethys*, *2023*20, 1–20. https://doi.org/10.3369/TETHYS.2023.20.01

Manwell, J. F., Mcgowan, J. G., & Rogers, A. L. 2009. *WIND ENERGY EXPLAINED THEORY, DESIGN AND APPLICATION* 2nd ed., Vol. 41, Issue 2. John Wiley & Sons, Ltd. www.wiley.com/go/wind_energy

Mas'ud, A. A., Wirba, A. V., Ardila-Rey, J. A., Albarracín, R., Muhammad-Sukki, F., Duque, Á. J., Bani, N. A., & Munir, A. B. 2017. Wind Power Potentials in Cameroon and Nigeria: Lessons from South Africa. *Energies 2017, Vol. 10, Page 443*, *10*4, 443. https://doi.org/10.3390/EN10040443

Mehta, M., Zaaijer, M., & Von Terzi, D. 2024. Drivers for optimum sizing of wind turbines for offshore wind farms. *Wind Energy Science*, *9*1, 141–163. https://doi.org/10.5194/WES-9-141-2024,

Mentis, D. 2013. *Wind Energy Assessment in Africa; A GIS-based approach* [KTH School of Industrial Engineering and Management]. https://urn.kb.se/resolve?urn=urn:nbn:se:kth:diva-125744

Minola, L., Zhang, F., Azorin-Molina, C., Pirooz, A. A. S., Flay, R. G. J., Hersbach, H., & Chen, D. 2020. Near-surface mean and gust wind speeds in ERA5 across Sweden: towards an improved gust parametrization. *Climate Dynamics*, *55*3–4, 887–907. https://doi.org/10.1007/S00382-020-05302-6/FIGURES/15

Motta, M., Barthelmie, R. J., & Vølund, P. 2005. The influence of non-logarithmic wind speed profiles on potential power output at danish offshore sites. *Wind Energy*, *8*2, 219–236. https://doi.org/10.1002/WE.146

Murcia, J. P., Koivisto, M. J., Luzia, G., Olsen, B. T., Hahmann, A. N., Sørensen, P. E., & Als, M. 2022. Validation of European-scale simulated wind speed and wind generation time series. *Applied Energy*, *305*, 117794. https://doi.org/10.1016/J.APENERGY.2021.117794

Mzough, oranderen M., & King Ededem, E. 2023. *ASSESSMENT OF WIND ENERGY RESOURCE AND POWER PRODUCTION ESTIMATES: A CASE STUDY OF CALABAR, SOUTH EASTERN NIGERIA*. https://doi.org/10.14293/PR2199.000029.V1

Nefabas, K. L., Söder, L., Mamo, M., & Olauson, J. 2021. Modeling of Ethiopian Wind Power Production Using ERA5 Reanalysis Data. *Energies 2021, Vol. 14, Page 2573*, *14*9, 2573. https://doi.org/10.3390/EN14092573

Nfaoui, H., Buret, J., & Sayigh, A. A. M. 1998. Wind characteristics and wind energy

potential in Morocco. *Solar Energy*, *63*1, 51–60. https://doi.org/10.1016/S0038-092X9800040-1

Nhamo, G., Chapungu, L., & Mutanda, G. W. 2025. Trends and impacts of climate-induced extreme weather events in South Africa 1920–2023. *Environmental Development*, *55*, 101183. https://doi.org/10.1016/J.ENVDEV.2025.101183

Pasqualetti, M., Righter, R., & Gipe, P. 2004. History of Wind Energy. In C. Cleveland Ed., *Encyclopedia of Energy* pp. 419–433. ACADEMIC PRESS. https://www.researchgate.net/publication/265594973_History_of_Wind_Energy#fullTextFileContent

Perkins, S. E., Pitman, A. J., Holbrook, N. J., & McAneney, J. 2007. Evaluation of the AR4 Climate Models' Simulated Daily Maximum Temperature, Minimum Temperature, and Precipitation over Australia Using Probability Density Functions. *Journal of Climate*, *20*17, 4356–4376. https://doi.org/10.1175/JCLI4253.1

Pichugina, Y. L., Banta, R. M., Brewer, W. A., Sandberg, S. P., & Hardesty, R. M. 2012. Doppler Lidar–Based Wind-Profile Measurement System for Offshore Wind-Energy and Other Marine Boundary Layer Applications. *Journal of Applied Meteorology and Climatology*, *51*2, 327–349. https://doi.org/10.1175/JAMC-D-11-040.1

Pouget, M. 2019. *Africa's energy access challenge: the role of AREI*. extension://mjdgandcagmikhlbjnilkmfnjeamfikk/https://www.germanclimatefinance.de/files/2019/07/AREI-–-About-the-Africa-Renewable-Energy-Initiative.pdf

Pryor, S. C., Shepherd, T. J., & Barthelmie, R. J. 2018. Interannual variability of wind climates and wind turbine annual energy production. *Wind Energy Science*, *3*2, 651–665. https://doi.org/10.5194/WES-3-651-2018,

Rashad, A., Kamel, S., & Jurado, F. 2017. The Basic Principles of Wind Farms. In *Distributed Generation Systems: Design, Operation and Grid Integration* 1st ed., pp. 21–67. Butterworth-Heinemann. https://doi.org/10.1016/B978-0-12-804208-3.00002-9

Rehman, S., & Al-Abbadi, N. M. 2005. Wind shear coefficients and their effect on energy production. *Energy Conversion and Management*, *46*15–16, 2578–2591. https://doi.org/10.1016/J.ENCONMAN.2004.12.005

Ridal, M., Bazile, E., Le Moigne, P., Randriamampianina, R., Schimanke, S., Andrae, U., Berggren, L., Brousseau, P., Dahlgren, P., Edvinsson, L., El-Said, A., Glinton, M.,

Hagelin, S., Hopsch, S., Isaksson, L., Medeiros, P., Olsson, E., Unden, P., & Wang, Z. Q. 2024. CERRA, the Copernicus European Regional Reanalysis system. *Quarterly Journal of the Royal Meteorological Society*, *150*763, 3385–3411. https://doi.org/10.1002/QJ.4764;SUBPAGE:STRING:FULL

Righter, R. W. . 1996. *Wind energy in America : a history*. University of Oklahoma Press.

Ryberg, D. S., Caglayan, D. G., Schmitt, S., Linßen, J., Stolten, D., & Robinius, M. 2019a. The future of European onshore wind energy potential: Detailed distribution and simulation of advanced turbine designs. *Energy*, *182*, 1222–1238. https://doi.org/10.1016/J.ENERGY.2019.06.052

Ryberg, D. S., Caglayan, D. G., Schmitt, S., Linßen, J., Stolten, D., & Robinius, M. 2019b. The future of European onshore wind energy potential: Detailed distribution and simulation of advanced turbine designs. *Energy*, *182*, 1222–1238. https://doi.org/10.1016/J.ENERGY.2019.06.052

Saha, S., Moorthi, S., Pan, H. L., Wu, X., Wang, J., Nadiga, S., Tripp, P., Kistler, R., Woollen, J., Behringer, D., Liu, H., Stokes, D., Grumbine, R., Gayno, G., Wang, J., Hou, Y. T., Chuang, H. Y., Juang, H. M. H., Sela, J., … Goldberg, M. 2010. The NCEP Climate Forecast System Reanalysis. *Bulletin of the American Meteorological Society*, *91*8, 1015–1058. https://doi.org/10.1175/2010BAMS3001.1

Sempreviva, A. M., Barthelmie, R. J., & Pryor, S. C. 2008. Review of methodologies for offshore wind resource assessment in European seas. *Surveys in Geophysics*, *29*6, 471–497. https://doi.org/10.1007/S10712-008-9050-2/FIGURES/7

Şen, Z. 2013. Modified wind power formulation and its comparison with Betz limits. *International Journal of Energy Research*, *37*8, 959–963. https://doi.org/10.1002/ER.2900;PAGEGROUP:STRING:PUBLICATION

Şen, Z., Altunkaynak, A., & Erdik, T. 2012. Wind Velocity Vertical Extrapolation by Extended Power Law. *Advances in Meteorology*, *2012*1, 178623. https://doi.org/10.1155/2012/178623

Skamarock, A. W., Klemp, A. J., Dudhia, A. J., Gill, A. D. O., Barker, A. D., Duda, A. M. G., Huang, A. X.-Y., Wang, A. W., Powers, A. J. G., & MMM, C. U. C. F. A. R. UCAR:National C. for A. R. NCAR:NCAR E. S. L. NESL:Mesoscale and M. M. D. 2008. *A Description of the Advanced Research WRF Version 3* p. 113. NCAR Tech. Note NCAR/TN-475+STR. https://doi.org/10.5065/D68S4MVH

Slivinski, L. C., Compo, G. P., Whitaker, J. S., Sardeshmukh, P. D., Giese, B. S., McColl, C., Allan, R., Yin, X., Vose, R., Titchner, H., Kennedy, J., Spencer, L. J., Ashcroft, L., Brönnimann, S., Brunet, M., Camuffo, D., Cornes, R., Cram, T. A., Crouthamel, R., … Wyszyński, P. 2019. Towards a more reliable historical reanalysis: Improvements for version 3 of the Twentieth Century Reanalysis system. *Quarterly Journal of the Royal Meteorological Society*, *145*724, 2876–2908. https://doi.org/10.1002/QJ.3598

Spera, D. A. 1994. *Wind Turbine Technology: Fundamental Concepts of Wind Turbine Engineering* 1st ed.. ASME Press.

Sterl, S., Liersch, S., Koch, H., Lipzig, N. P. M. V., & Thiery, W. 2018. A new approach for assessing synergies of solar and wind power: Implications for West Africa. *Environmental Research Letters*, *13*9. https://doi.org/10.1088/1748-9326/aad8f6

Stuecker, M. F. 2023. The climate variability trio: stochastic fluctuations, El Niño, and the seasonal cycle. *Geoscience Letters 2023 10:1*, *10*1, 1–19. https://doi.org/10.1186/S40562-023-00305-7

Taylor, K. E. 2001. Summarizing multiple aspects of model performance in a single diagram. *Journal of Geophysical Research Atmospheres*, *106*D7, 7183–7192. https://doi.org/10.1029/2000JD900719;WGROUP:STRING:PUBLICATION

Thomas, R. L., & Robbins, W. H. 1980. Large wind-turbine projects in the United States wind energy program. *Journal of Wind Engineering and Industrial Aerodynamics*, *5*3–4, 323–335. https://doi.org/10.1016/0167-61058090040-9

Tizgui, I., Bouzahir, H., Guezar, F. El, & Benaid, B. 2018. Wind speed extrapolation and wind power assessment at different heights. *Proceedings of 2017 International Conference on Electrical and Information Technologies, ICEIT 2017*, 1–4. https://doi.org/10.1109/EITECH.2017.8255215

Tolasa, D. G., & Furi, A. T. 2025. The Role of Advanced Materials in the Optimization of Wind Energy Systems: A Physics Based Approach. *Acceleron Aerospace Journal*, *4*1, 847–857. https://doi.org/10.61359/11.2106-2504

Trisos, C. H., Adelekan, I. O., Totin, E., Ayanlade, A., Efitre, J., Gemeda, A., Kalaba, K., Lennard, C., Masao, C., Mgaya, Y., Ngaruiya, G., Olago, D., Simpson, N. P., & Zakieldeen, S. 2022. Africa. In H.-O. Pörtner, D. C. Roberts, M. Tignor, E. S. Poloczanska, K. Mintenbeck, A. Alegría, M. Craig, S. Langsdorf, S. Löschke, V.

Möller, A. Okem, & B. Rama Eds., *Climate Change 2022: Impacts, Adaptation and Vulnerability. Contribution of Working Group II to the Sixth Assessment Report of the Intergovernmental Panel on Climate Change* pp. 1285–1455. Cambridge University Press. https://doi.org/10.1017/9781009325844.011

Tumse, S., Bilgili, M., Yildirim, A., & Sahin, B. 2024. Comparative Analysis of Global Onshore and Offshore Wind Energy Characteristics and Potentials. *Sustainability*, *16*15, 6614. https://doi.org/10.3390/SU16156614

Wan, J., Liu, J., Ren, G., Guo, Y., Hao, W., Yu, J., & Yu, D. 2019. A universal power-law model for wind speed uncertainty. *Cluster Computing*, *22*4, 10347–10359. https://doi.org/10.1007/S10586-017-1350-1/FIGURES/24

Wharton, S., & Lundquist, J. K. 2012. Atmospheric stability affects wind turbine power collection. *Environmental Research Letters*, *7*1, 014005. https://doi.org/10.1088/1748-9326/7/1/014005

Wind Atlas for South Africa. 2010. *Wind Speeds Observed Data.* Installed Meteorological Masts for the WASA Project [Dataset]. http://wasadata.csir.co.za/wasa1/WASAData

World Meteorological Organization. 2019. Manual on Codes - International Codes. In *WMO Technical Regulations: Vol. I.1* 2019th ed., Issue 306, p. 463. World Meteorological Organization.

Xu, C., Hao, C., Li, L., Han, X., Xue, F., Sun, M., & Shen, W. 2018a. Evaluation of the Power-Law Wind-Speed Extrapolation Method with Atmospheric Stability Classification Methods for Flows over Different Terrain Types. *Applied Sciences 2018, Vol. 8, Page 1429*, *8*9, 1429. https://doi.org/10.3390/APP8091429

Xu, C., Hao, C., Li, L., Han, X., Xue, F., Sun, M., & Shen, W. 2018b. Evaluation of the Power-Law Wind-Speed Extrapolation Method with Atmospheric Stability Classification Methods for Flows over Different Terrain Types. *Applied Sciences 2018, Vol. 8, Page 1429*, *8*9, 1429. https://doi.org/10.3390/APP8091429

Zängl, G., Reinert, D., Rípodas, P., & Baldauf, M. 2015. The ICON ICOsahedral Non-hydrostatic modelling framework of DWD and MPI-M: Description of the non-hydrostatic dynamical core. *Quarterly Journal of the Royal Meteorological Society*, *141*687, 563–579. https://doi.org/10.1002/QJ.2378

Zheng, X., Yao, Y., Hu, Z., Yu, Z., & Hu, S. 2022. Influence of Turbulence Intensity on the Aerodynamic Performance of Wind Turbines Based on the Fluid-Structure

Coupling Method. *Applied Sciences 2023, Vol. 13, Page 250*, *13*1, 250. https://doi.org/10.3390/APP13010250

Zou, M., & Djokic, S. Z. 2020. A Review of Approaches for the Detection and Treatment of Outliers in Processing Wind Turbine and Wind Farm Measurements. *Energies 2020, Vol. 13, Page 4228*, *13*16, 4228. https://doi.org/10.3390/EN13164228

APPENDICES

Table 14: Summary of data used

Datasets	Labels	Sources
OBSERVED	TAHMO	https://tahmo.org/
	SASSCAL_WN	https://sasscalweathernet.org/
	NCEI_ISD	https://www.ncei.noaa.gov/products/land-based-station/integrated-surface-database
	WASA	https://wasadata.csir.co.za/wasa1/WASAData
ERA5	All	https://cds.climate.copernicus.eu/datasets/reanalysis-era5-single-levels?tab=overview
GWA	All	https://globalwindatlas.info/en/
ICON-LAM	All	https://doi.org/10.26165/JUELICH-DATA/JYGQ65

Table 15 : Summary of wind speed scaling results

		20 m				40 m				60 m			
		MAE	ME	Pearson r	PSS	MAE	ME	Pearson r	PSS	MAE	ME	Pearson r	PSS
Obs_extra	1_7_Law	0.353	-0.043	0.995	0.982	0.820	-0.011	0.976	0.952	1.151	-0.094	0.955	0.944
	Counihan_Law	0.363	-0.080	0.995	0.983	0.799	-0.060	0.976	0.953	1.133	-0.075	0.955	0.943
	Justus_Law	0.423	0.264	0.995	0.959	1.035	0.635	0.975	0.919	1.440	0.886	0.951	0.898
	Khalfa_Law	0.435	0.018	0.994	0.944	0.879	0.071	0.971	0.896	1.314	0.158	0.944	0.861
	LogLaw	0.365	0.059	0.995	0.972	0.879	0.167	0.976	0.955	1.213	0.182	0.955	0.945
	Nfaoui_Law	0.365	-0.006	0.995	0.968	0.823	0.107	0.975	0.943	1.165	0.155	0.951	0.921
	Spera_Law	0.360	0.140	0.995	0.968	0.888	0.379	0.976	0.932	1.244	0.529	0.951	0.919
ERA5_GWA	1_7_Law	1.808	-0.121	0.819	0.929	2.004	-0.191	0.795	0.932	2.204	-0.214	0.765	0.926
	Counihan_Law	1.787	-0.229	0.819	0.931	2.028	-0.366	0.795	0.928	2.233	-0.456	0.765	0.916
	Justus_Law	1.596	0.169	0.817	0.923	1.779	0.469	0.793	0.911	2.061	0.742	0.763	0.910
	Khalfa_Law	1.608	0.037	0.815	0.918	1.756	-0.067	0.787	0.901	1.894	-0.200	0.759	0.882
	LogLaw	1.782	-0.088	0.819	0.929	1.984	-0.117	0.795	0.931	2.168	-0.186	0.765	0.932
	Nfaoui_Law	1.700	-0.066	0.817	0.929	1.846	-0.138	0.793	0.922	1.970	-0.141	0.763	0.910
	Spera_Law	1.680	-0.002	0.817	0.922	1.805	0.172	0.794	0.921	1.952	0.265	0.763	0.924
ICON-LAM	1_7_Law	1.626	-0.091	0.814	0.949	1.874	-0.168	0.772	0.942	2.107	-0.141	0.754	0.942
	Counihan_Law	1.623	-0.134	0.814	0.953	1.851	-0.327	0.772	0.946	2.099	-0.348	0.754	0.947
	Justus_Law	1.626	0.205	0.813	0.944	1.856	0.485	0.769	0.934	2.097	0.805	0.747	0.916

	Khalfa_Law	1.574	-0.003	0.810	0.943	1.687	-0.058	0.762	0.925	1.873	-0.070	0.734	0.900
	LogLaw	1.607	-0.020	0.814	0.953	1.859	-0.145	0.772	0.943	2.121	-0.134	0.754	0.939
	Nfaoui_Law	1.591	-0.043	0.813	0.953	1.763	-0.128	0.769	0.945	1.945	0.005	0.747	0.937
	Spera_Law	1.596	0.073	0.813	0.950	1.743	0.117	0.769	0.953	2.004	0.295	0.748	0.945
	Adv_Lin	1.968	-1.064	0.795	0.905	1.663	-0.346	0.801	0.942	2.169	-0.961	0.763	0.899
	Adv_Pl	1.574	-0.046	0.821	0.955	1.616	-0.080	0.802	0.957	1.748	0.017	0.796	0.952
	Adv_Log	1.608	-0.017	0.814	0.953	1.639	-0.075	0.801	0.956	1.758	0.101	0.795	0.955
ERA5	1_7_Law	2.669	-1.201	0.819	0.825	2.643	-1.528	0.795	0.813	3.074	-1.724	0.765	0.812
	Counihan_Law	2.701	-1.240	0.819	0.821	2.701	-1.614	0.795	0.806	3.155	-1.789	0.765	0.795
	Justus_Law	2.423	-0.897	0.817	0.822	2.188	-0.838	0.793	0.857	2.358	-0.743	0.763	0.865
	Khalfa_Law	2.521	-1.006	0.815	0.806	2.381	-1.165	0.788	0.810	2.616	-1.210	0.760	0.805
	LogLaw	2.617	-1.141	0.819	0.831	2.587	-1.444	0.795	0.825	3.026	-1.642	0.765	0.815
	Nfaoui_Law	2.582	-1.093	0.817	0.811	2.460	-1.378	0.793	0.808	2.753	-1.593	0.763	0.798
	Spera_Law	2.520	-1.019	0.817	0.824	2.355	-1.073	0.794	0.829	2.606	-1.192	0.763	0.851
	Adv_Lin	3.566	-2.224	0.809	0.700	2.823	-1.746	0.809	0.759	2.884	-1.577	0.816	0.790
	Adv_Pl	2.651	-1.312	0.819	0.803	2.559	-1.219	0.819	0.807	2.711	-1.364	0.821	0.813
	Adv_Log	2.729	-1.386	0.816	0.810	2.569	-1.339	0.815	0.810	2.749	-1.412	0.819	0.809